



Deposited via The University of Sheffield.

White Rose Research Online URL for this paper:

<https://eprints.whiterose.ac.uk/id/eprint/134046/>

Version: Accepted Version

---

**Article:**

Heath, P.G., Corkhill, C.L., Stennett, M.C. et al. (2018) Immobilisation of Prototype Fast Reactor raffinate in a barium borosilicate glass matrix. *Journal of Nuclear Materials*, 508. pp. 203-211. ISSN: 0022-3115

<https://doi.org/10.1016/j.jnucmat.2018.05.015>

---

**Reuse**

This article is distributed under the terms of the Creative Commons Attribution-NonCommercial-NoDerivs (CC BY-NC-ND) licence. This licence only allows you to download this work and share it with others as long as you credit the authors, but you can't change the article in any way or use it commercially. More information and the full terms of the licence here: <https://creativecommons.org/licenses/>

**Takedown**

If you consider content in White Rose Research Online to be in breach of UK law, please notify us by emailing [eprints@whiterose.ac.uk](mailto:eprints@whiterose.ac.uk) including the URL of the record and the reason for the withdrawal request.

1

## 2 **Immobilisation of Prototype Fast Reactor Raffinate using Barium**

### 3 **Silicate ILW Glasses**

4 Paul G. Heath, Claire L. Corkhill, Martin C. Stennett, Russell J. Hand, Kieran M. Whales, Neil C.  
5 Hyatt

6 Immobilisation Science Laboratory, Sir Robert Hadfield Building, Mappin Street, The  
7 University of Sheffield, Sheffield, S1 3JD, United Kingdom

#### 8 **Abstract**

9 The vitrification of Dounreay Prototype Fast Reactor Raffinate (PFR) in a barium borosilicate  
10 glass matrix was investigated, with the aim of understanding process feasibility and the  
11 potential benefits over the current baseline of cement encapsulation. Laboratory scale glass  
12 melts demonstrated the production of homogeneous glasses incorporating at least 20 wt%  
13 simulant PFR waste (on an oxides basis), with no detectable crystalline accessory phases. The  
14 hardness and indentation fracture toughness of the simulant PFR waste glasses were  
15 determined to be comparable to those of current UK high level waste glass formulations. The  
16 normalised dissolution rate of boron from the simulant PFR glasses was determined to be  $3 \times$   
17  $10^{-2} \text{ g m}^{-2} \text{ d}^{-1}$ , in  $18.2 \text{ M}\Omega$  water at  $90^\circ\text{C}$  and surface area / volume ratio of  $1500 \text{ m}^{-1}$ ; only a  
18 factor of two greater than the French SON-68 simulant high level waste glass, under  
19 comparable conditions. Consequently, the simulant PFR waste glasses are considered to  
20 show considerable promise for meeting envisaged waste acceptance criteria for geological  
21 disposal. Overall, the superior stability of vitrified PFR wasteforms could enhance the safety

- 22 case for long term near surface storage of radioactive wastes, mandated by current Scottish
- 23 Government policy.
- 24 Keywords: Amorphous Materials, Waste Immobilisation, Mechanical properties.

## 25 Introduction

26 The Prototype Fast Reactor (PFR) was the UK's second fast reactor and operated between  
27 1974 and 1994, utilising a high plutonium content mixed oxide fuel (MOx) with a molten  
28 sodium coolant [1]. Spent fuel from the PFR was reprocessed on the Dounreay site by  
29 dissolution in nitric acid to recover the reusable fissile material. This process yielded  
30 approximately 200 m<sup>3</sup> of an aqueous radioactive liquor, known as PFR raffinate [2]. The PFR  
31 raffinate contains the majority of the radioactive material and fission products produced  
32 during the operation of the PFR reactor and on the Dounreay site as a whole [3]. Since the  
33 reprocessing of PFR fuel was completed in 1996, the waste raffinate has been stored in  
34 underground tanks on the Dounreay site. Having spent a decade in storage, PFR raffinate was  
35 reclassified as Intermediate Level Waste in 2004, ostensibly due to its low heat output [4].

36 The conditioning of PFR raffinate into a passively safe, wasteform is identified as a priority in  
37 the Dounreay Site Restoration Plan [5]. A best practical environmental option assessment,  
38 undertaken by the UKAEA, proposed neutralisation and cementation of the raffinate as the  
39 reference waste management strategy [6]. For this waste treatment option to be  
40 implemented, a new facility (to be known as D3900) is required, the construction of which is  
41 yet to begin at the time of writing.

42 Although laboratory studies have demonstrated that cement-encapsulated *inactive* raffinate  
43 has physical properties comparable to those of other cemented ILW streams (e.g. viscosity,  
44 initial setting time, bleed water), PFR raffinate has a specific activity 20 times greater than  
45 other encapsulated ILW streams [2,3,7,8]. The high concentration of <sup>137</sup>Cs in PFR raffinates,  
46 the porous nature and poor immobilisation of Cs observed in cementitious systems, may limit  
47 the ability of cement to retain the radioactive inventory of PFR [2,9-11]. It is not yet certain  
48 that environmental release rates from a cemented PFR raffinate wasteform will be within

49 permitted limits over the relevant lifetime of the wastefrom, particularly given the policy of  
50 the Scottish Government for long term near-surface storage at a coastal location, as in the  
51 case of Dounreay [12,13].

52 An issue that may be even more significant to safe interim storage is the high specific activity  
53 of the wastes and their significant alpha emitting component ( $\beta/\gamma = 346 \text{ TBq m}^{-3}$ ,  $\alpha = 3.21$   
54  $\text{TBq m}^{-3}$ ) [2]. It is known that the radiolysis of cementitious water will produce  $\text{H}_2$ , while the  
55 presence of significant nitrate concentrations in the waste ( $300\text{-}500 \text{ g l}^{-1}$ ) and alpha activity  
56 will also result in the formation of  $\text{O}_2$  and  $\text{NO}_x$  [14–17]. These combined factors will increase  
57 the rate of gas generation when compared to existing UK ILW waste packages. As a result,  
58 these reactions could be expected to introduce significant complexities to the long-term  
59 management of cemented PFR raffinate waste packages through the need to monitor, vent  
60 and dissipate gases from the waste packages.

61 It should be noted that the near-surface storage policy was introduced after the strategic  
62 decision to encapsulate PFR raffinates in a cement wastefrom. In its response to the Scottish  
63 Government consultation on higher activity wastes, the Committee on Radioactive Waste  
64 Management (CoRWM) highlighted that certain wastes from the Dounreay site were “*never*  
65 *likely to be suitable for near surface disposal and therefore greater efforts need to be made in*  
66 *the interest of safety, security and intergenerational equity to find a permanent solution for*  
67 *this waste*” [12].

68 The current investigation aims to demonstrate, in principle, an alternative processing option  
69 for PFR raffinate, which could enhance the safety case for long term near-surface storage and  
70 address the concerns of CoRWM. A derivative of the barium borosilicate glass, G73, previously  
71 investigated as a matrix for the immobilisation of UK ILWs arising at Magnox decommissioning  
72 sites [18-21], is here investigated as a disposal matrix for PFR raffinate, the composition of

73 which incorporates ca. 7 wt% SO<sub>3</sub>. Barium borosilicate glasses, such as G73, are reported to  
74 have a high aqueous durability and the presence of Ba is known to increase the solubility of  
75 sulphate species, which inhibits the formation of water soluble “yellow phase” salts [18-23].  
76 We present an analysis of the composition, amorphous nature, aqueous durability, thermal  
77 behaviour and mechanical properties of vitrified PFR raffinate with waste loadings of 10 wt%,  
78 15 wt% and 20 wt% (oxide basis), in a barium borosilicate glass. The results are discussed with  
79 reference to the potential benefits of PFR raffinate vitrification compared to cementation.

## 80 **2 - Materials and Experimental**

### 81 **2.1 - Materials**

#### 82 **2.1.1 Raffinate Simulant**

83 The inactive surrogate for PFR raffinate was formulated on the assumption that the waste  
84 would be treated using an evaporation or calcination step to produce a solid calcine prior to  
85 vitrification. The composition was thus formulated using the data available on the average  
86 composition of four PFR tanks at the Dounreay site [6]. **The chemical composition of model**  
87 **PFR raffinate is provided in Table 1. The solids content of the raffinate calcine was calculated**  
88 **based on the reported elemental values in the raffinate (ppm) and then converted to their**  
89 **oxide form, which is reported in Table 2.**

90 **Some variations in the elemental composition were necessary when batching the simulant.**  
91 **For example, for reasons of practicality, any elements with concentrations < 15 ppm were**  
92 **excluded** (Ag, As, Cm, Dy, Eu, Gd, Ge, Hg, Ho, In, Nb, Np, P, Pb, Pd, Rb, Rh, Sb, Se, Sn and Tc).  
93 One exception was Pd, which was present at a concentration of ~150 ppm in the waste

94 stream. This was excluded on grounds of cost, for this preliminary study, and its known  
95 propensity to exist as an insoluble noble metal in glass melts [24].

96 The omission of **the elements noted above accounted** for < 2.8 wt% of the mass of the total  
97 waste stream. Radioactive elements with concentrations > **15 ppm** were substituted by  
98 relevant concentrations of inactive surrogates (Ce for U and Sm for Am).

### 99 **2.1.2 Glass Preparation**

100 Three glasses were synthesised and characterised in this study. These glasses were based on  
101 a derivative of the G73 barium-silicate base glass composition (referred to here as G73, for  
102 simplicity), which was previously developed [18-21], with PFR raffinate simulant incorporated  
103 at 10 wt%, 15 wt% and 20 wt% waste loading. These glasses are identified as G73-10, G73-15  
104 and G73-20, respectively. The base glass composition, presented in Table 2 for reference, is  
105 identified as G73-00.

106 Glasses were produced from batch chemicals to provide 250 g of glass. The components of  
107 the raffinate simulant were batched in either their oxide or carbonate forms according to  
108 their molar proportions to obtain the specified waste loading. The following analytical grade  
109 chemicals were used for batching; Al(OH)<sub>3</sub>, Na<sub>2</sub>B<sub>4</sub>O<sub>7</sub>·10H<sub>2</sub>O, BaCO<sub>3</sub>, CaCO<sub>3</sub>, CdO, CeO<sub>2</sub>,  
110 Cr(NO<sub>3</sub>)<sub>3</sub>·9H<sub>2</sub>O, Cs<sub>2</sub>CO<sub>3</sub>, CuO, Fe<sub>2</sub>O<sub>3</sub>, La<sub>2</sub>O<sub>3</sub>, Mn<sub>2</sub>O<sub>3</sub>, MoO<sub>3</sub>, Na<sub>2</sub>CO<sub>3</sub>, Nd<sub>2</sub>O<sub>3</sub>, NiCO<sub>3</sub>, Pr<sub>6</sub>O<sub>11</sub>, RuO<sub>2</sub>,  
111 Na<sub>2</sub>SO<sub>4</sub>, SiO<sub>2</sub>, Sm<sub>2</sub>O<sub>3</sub>, SrCO<sub>3</sub>, TeO<sub>2</sub>, TiO<sub>2</sub>, Y<sub>2</sub>O<sub>3</sub> and ZnO. The batched powders were heated in  
112 mullite crucibles with stirring to 1200 °C at 10 °C min<sup>-1</sup> and held at temperature for 3 hours.  
113 The glasses were poured into blocks and annealed at 500 °C for one hour before cooling to  
114 25 °C at 1 °C min<sup>-1</sup>. Glass monoliths were prepared for SEM-EDX, Vickers hardness testing and  
115 fracture toughness testing to a 0.25 µm finish by successive grinding and polishing with SiC  
116 grit papers and diamond pastes. Powder samples were prepared using a hardened steel ring

117 and puck mill. The sub-75  $\mu\text{m}$  size fraction was collected for use in XRD and XRF analysis and  
118 the 75-150  $\mu\text{m}$  size fraction was collected for use in aqueous durability experiments and  
119 prepared according to ASTM standard C 1285 – 02 [25].

## 120 **2.2 - Characterisation**

### 121 **Glass Characterisation**

122 X-ray Fluorescence (XRF) analysis was performed using a Phillips PW2404 XRF Axios  
123 instrument to obtain compositional data.  $\text{B}_2\text{O}_3$  content was determined by dissolution of glass  
124 powder in HF followed by analysis of leachate using a Perkin-Elmer Optima 5300 dual view  
125 Inductively Coupled Plasma Atomic Emission Spectroscopy (ICP-AES). The density of the glass  
126 wastefoms was measured using a  $< 75 \mu\text{m}$  powder, using an AccuPyc 1340 II helium  
127 pycnometer with the following analysis regime; 200 purges of the chamber followed by 50  
128 cycles using an equilibration rate of  $35 \text{ Pa min}^{-1}$  at  $25 \text{ }^\circ\text{C}$  in a  $1 \text{ cm}^3$  chamber and a fill pressure  
129 of 86.2 KPa. Scanning Electron Microscopy was performed using a JEOL JSM 6400 SEM with  
130 an accelerating voltage of 20 kV and a working distance of 15 mm. Concurrent Energy  
131 Dispersive Spectroscopy was acquired (INCA, Oxford Instruments). Additionally, an FEI  
132 Quanta 200 F SEM was utilised for high resolution imaging, using an accelerating voltage of  
133 30 kV and working distance of 10 mm. Concurrent Energy Dispersive X-ray analysis was  
134 performed (Genesis EDX).

### 135 **Thermal and mechanical properties**

136 The glass liquidus temperature for each sample was measured by placing a 20 cm long mullite  
137 boat, filled with sub-75  $\mu\text{m}$  glass powder, into a tube furnace. The samples were left to  
138 equilibrate at  $1200 \text{ }^\circ\text{C}$  for 24 hours and the temperature gradient along the length of the boat  
139 at 5 mm intervals was measured using a retractable thermocouple. The boats were removed

140 and rapidly quenched in air. The point of crystallisation was measurable to within 1 mm by  
141 optical examination of the crucibles and this was then correlated with the associated  
142 temperature to estimate the liquidus temperature. Alterations in chemical composition  
143 resulting from crucible corrosion were not accounted for, nor were the phases produced  
144 analysed. As the purpose of this test was to check if the point of crystallisation was below  
145 1100 °C, and the contaminants from crucible corrosion are likely to lower this value, the  
146 results presented are considered useful in this context.

147 The Vickers hardness indentation method was used to determine both hardness ( $H_v$ ) and the  
148 indentation fracture toughness ( $K_C$ ) following the procedure described by Connelly et al. [26].  
149 Indentation was performed on a Mitutayo HM-101. Sixty indents were made at each of three  
150 indentation loadings; 0.98 N, 1.96 N and 2.94 N (twenty indents at each force per sample,  
151 error  $\pm 0.02$  N). The load was held for 20 seconds. Samples were left for 24 hours prior to  
152 analysis using optical microscopy. The Vickers hardness ( $H_v$ ) in Pa and the Fracture Toughness  
153 ( $K_C$ ) was calculated using Equations 1 and 2 respectively:

$$154 \quad H_v = \frac{1.854P}{(2a)^2} \quad \text{Equation 1}$$

$$155 \quad K_C = \frac{0.0824P}{c^{3/2}} \quad \text{Equation 2}$$

156 where  $P$  is the applied load (N),  $a$  is the half length of the indent diagonal (m) and  $c$  is the  
157 median/radial crack length (m). The results quoted are those obtained from the 1.96 N  
158 loading due to the higher number of acceptable indentations (a minimum of fifteen per  
159 sample).

160 **Aqueous durability assessment**

161 Aqueous durability assessment was performed according to ASTM standard C 1285 - 02  
162 (Product Consistency Test - PCT) utilising a 75 µm - 150 µm size fraction in 18.2 MΩ H<sub>2</sub>O at  
163 90°C with a SA/V between 1499 m<sup>-1</sup> and 1525 m<sup>-1</sup> dependent on glass density, as provided in  
164 Table 3 [25]. Experiments were performed in triplicate with duplicate blanks, sampling at 3,  
165 7, 14, 21 and 28 days. Samples were filtered using a 0.45 µm PTFE filter and leachate analysis  
166 was performed using ICP-AES.

167 The normalised elemental mass loss (NL<sub>i</sub>) and normalised elemental dissolution rates (NR<sub>i</sub>)  
168 were calculated according to Equations 3 and 4, respectively; using the analysed glass  
169 compositions.

170 
$$NL_i = \frac{C_i}{f_i \times \frac{SA}{V}}$$
 **Equation 3**

171 
$$NR_i = \frac{C_i}{f_i \times \frac{SA}{V} \times t}$$
 **Equation 4**

172 where NL<sub>i</sub> is the normalised elemental mass loss of element *i* (g m<sup>-2</sup>), C<sub>i</sub> is the averaged, blank  
173 corrected concentration of element *i* in solution (g m<sup>-3</sup>), f<sub>i</sub> is the fraction of element *i* in the  
174 unleached glass, SA/V is the ratio of glass surface area to the volume of water (m<sup>-1</sup>), NR<sub>i</sub> is the  
175 normalised elemental loss rate and t is time in days.

176 Geochemical modelling of the solution leachate was performed using the Phreeqc  
177 geochemical modelling code (v3-12-8538, provided by the United States Geological Survey)  
178 to identify solution saturation species, using the Lawrence Livermore National Laboratory  
179 (LLNL) thermodynamic database.

## 180 **3 - Results**

### 181 **3.1 - Glass Formation and Composition**

182 It can be stated with confidence that the three simulant PFR waste loaded G73 glasses exist  
183 within a stable glass forming region of the phase diagram up to a 20 wt% loading. The glasses  
184 formed readily and poured from the melt at 1200 °C, with no evidence of un-dissolved batch.  
185 However, a small degree of corrosion was evident inside the crucible, which is responsible for  
186 the elevated concentrations of alumina in the final composition. The composition of the three  
187 glasses was analysed using XRF and ICP-AES; data are shown in Table 2, which compares the  
188 final composition with the nominal batched compositions.

189 Overall, it can be seen from Table 2 that the batched and analysed compositions are in  
190 reasonable agreement for major and minor oxides, although with some notable exceptions.  
191 Na<sub>2</sub>O, B<sub>2</sub>O<sub>3</sub>, and SO<sub>3</sub>, are, in general, analysed as lower than the batched composition, due to  
192 volatilisation from the melts during high temperature processing. SiO<sub>2</sub> and BaO are,  
193 respectively, systematically higher and lower in the analysed glass compositions compared to  
194 the batched. The complexity of the glass composition made deconvolution of overlapping X-  
195 ray emission lines, from multiple elements, challenging and may be responsible for this  
196 systematic discrepancy. The loss of such volatile components from the melts does not pose  
197 a challenge to the off-gas system of existing HLW melter systems and, therefore, is not  
198 expected to be problematic for full scale deployment. In addition, it should be noted that the  
199 lower surface area to volume ratio, and presence of a cold cap, in full scale melter systems  
200 will reduce volatilisation considerably, with respect to laboratory scale melts.

201 Analysis of the vitrified products by X-ray diffraction showed only diffuse scattering (Figure 1)  
202 characteristic of an amorphous material, with no evidence of phase separation or detectable

203 crystallisation. The lack of contrast in both the SEM-BSE imaging and SEM-EDX mapping  
204 analysis, displayed in Figure 1b and Figure 2, is indicative of a chemically homogeneous glass  
205 on a micron scale. Each glass showed similar characteristics. There was no evidence from XRD  
206 or SEM-EDX analysis of distinct segregated sulphate phases.

207 Crystallisation in radioactive waste glasses, when produced from the melt, is undesirable for  
208 several reasons, including: the possibility for the precipitation of soluble radionuclide  
209 containing phases; the potential for decreased aqueous durability of the matrix, due to the  
210 removal of refractory components; and the potential for swelling of crystal phases as a result  
211 of damage from self-irradiation. The absence of significant crystallisation and minimal  
212 evidence of crucible corrosion indicate that a high-quality glass wastefrom was obtained that  
213 should be both stable and amenable to the processing of PFR wastes.

### 214 **3.2 - Thermal Properties**

215 Table 3 shows the density, glass transition temperature and measured liquidus temperature  
216 of the simulant PFR glasses. The values obtained for the  $T_g$  are comparable, within error, for  
217 the three waste-loadings and correspond well with the transition temperature previously  
218 reported for the same base glass loaded with organic exchange resins [18-21].

219 The liquidus temperatures of the glasses were all below 1100 °C, and no correlation with  
220 increasing waste loading was observed. Glass compositions with a liquidus temperature  
221 below 1100 °C are thought to be beneficial for nuclear waste vitrification as the lower  
222 temperatures minimise volatile losses of radioactive components during melting [27-29].

223 **Although not essential for all melter operations or wastefrom acceptance criteria, the**  
224 **absence of crystalline products indicates that the wastefroms will be amenable to commercial**

225 application; due to the associated simplification of wasteform qualification, improved  
226 efficiency of melter operation and predictability of process control [30]

227 As the glasses produced in this study have been shown to retain their Cs inventory after  
228 processing at 1200 °C, the retention of Cs should be expected to be retained in full scale melts  
229 given the smaller melt surface area to volume ratio and possibility of operating with a cold  
230 cap [31].

### 231 3.3 - Mechanical Testing

232 The Vickers hardness and indentation fracture toughness of the PFR simulant glasses are  
233 plotted in Figure 3. The fracture toughness of the glass relates to the energy required to form  
234 a new surface and is relevant to qualifying the suitability of radioactive waste packages for  
235 transport, e.g. in estimating the likelihood of respirable fines formation in accident scenario  
236 [32].

237 The lowest waste loaded glass, G73-10, had the highest indentation fracture toughness and  
238 the hardness value of the glasses tested. G73-15 and G73-20 glasses gave lower values and  
239 were equivalent within measurable precision. All compositions were comparable or superior  
240 to existing HLW glass compositions (e.g. UK MW glass and US PNL 76-78 glass, Fig. 3) for  
241 indentation fracture toughness and were comparable, or superior, in terms of Vickers  
242 hardness [26,32].

243 Although no specification for fracture toughness currently exists for UK vitreous waste  
244 packages, the results imply that, as the G73 based glasses are comparable to current  
245 wasteforms, they are likely to be compliant with storage in existing (HLW) canisters.  
246 Furthermore, the mechanical properties suggest that packaging in larger 3 m<sup>3</sup> boxes may also

247 be possible, although in this case analysis of thermally induced cracking/stresses during  
248 processing requires investigation.

### 249 3.4 - Aqueous Durability

250 The short-term chemical durability of the simulant raffinate glasses was investigated using  
251 the PCT methodology [25]. Figure 4 shows the normalised mass loss of elements that were  
252 detectable by ICP-AES in concentrations higher than those measured in the blank solutions.  
253 The normalised elemental mass loss ( $NL_i$ ) and normalised dissolution rate ( $NR_i$ , 28 days) data  
254 are shown in Tables 4 and 5, respectively. The solution pH buffered to a value of  $pH\ 10.2 \pm 0.2$   
255 after 3 days (Fig. 4) and there was no further measurable fluctuation of pH during the 28-day  
256 duration of the experiments.

257 The normalised elemental loss rates (to 28 days) for boron were similar for each glass  
258 composition, giving an  $NR_B$  between  $3.24 \times 10^{-2} \text{ g m}^{-2} \text{ d}^{-1}$  and  $3.33 \times 10^{-2} \text{ g m}^{-2} \text{ d}^{-1}$  ( $\pm 5 \times 10^{-4}$ )  
259 as stated in Table 4. This indicates that varying the waste loading from 10 to 20 wt% did not  
260 appreciably alter the chemical durability on the timescales investigated. Importantly, the  
261 glasses showed a comparable normalised mass loss and normalised dissolution rate to other  
262 high-level waste glass compositions destined for long-term disposal, tested under comparable  
263 conditions (Table 5). For example, the UK HLW MW25 glass, has a  $NR_B$  of  $3.20 \times 10^{-1} \text{ g m}^{-2} \text{ day}^{-1}$   
264 [33], compared with  $3.24 \times 10^{-2} \text{ g m}^{-2} \text{ d}^{-1}$  for the 20 wt% loaded simulant PFR raffinate glass  
265 (Table 5). The  $NR_B$  is approximately twice that of the SON68 French HLW base glass, however  
266 it should be noted that the specific activity in R7T7 (the active analogue of SON68) will be  
267 substantially higher than that of the PFR loaded G73 glasses. At production, R7T7 contains an  
268 average specific activity ca.  $110 \text{ PBq m}^{-3}$ , approximately 20 times greater than the average ca.

269 6 PBq m<sup>-3</sup> estimated for the G73-20 glass [34]. As such, these glasses could be considered  
270 suitable for the immobilisation and disposal of PFR raffinate.

271 Glass dissolution was observed to be incongruent; B and Na leached at similar rates ( $NL_B >$   
272  $NL_{Na}$ ), however the normalised mass loss of all other elements was an order of magnitude  
273 lower than both B and Na (Table 4). The normalised mass loss of all elements was observed  
274 to be rapid for the first 3 days of dissolution and, after this time, the normalised mass loss of  
275 Si, Na, B began to reduce indicating an approach to quasi-equilibrium, as indicated in Figure  
276 4.

277 The normalised mass loss of Ba and Ca differed as a function of glass composition, albeit  
278 without a notable trend. For example, the normalised mass loss of Ba decreased after 7 days  
279 for the 20 wt% waste loaded composition, and after 14 days for the 15 wt% glass (Fig. 4b).  
280 There appeared to be little removal of Ba from solution from the 10 wt% loaded glass.  
281 Additionally, the  $NL_{Sr}$  dropped after 14 days for all three glasses (Fig. 4f). This behaviour may  
282 be attributed to the formation of Ca-, Ba- and Sr-containing alteration layers on the glass  
283 surface. Indeed, geochemical modelling indicated that tobermorite ( $Ca_5Si_6H_{11}O_{22.5}$ ) is likely to  
284 precipitate. A number of recent investigations have also identified this phase in glasses  
285 containing Ca, or where Ca is present in solution [35–39] and have shown that its formation  
286 can significantly reduce the dissolution rate of nuclear waste glasses, by an order of  
287 magnitude compared to other media [39]. Other phases shown by geochemical modelling to  
288 be favourable precipitates were the Ca- Ba- and Sr-carbonate phases, calcite ( $CaCO_3$ ),  
289 witherite ( $BaCO_3$ ) and strontianite ( $SrCO_3$ ). Arising from equilibrium of  $CO_2$  in air with the  
290 leaching medium, it is possible that these phases precipitated in solution, and when the  
291 samples were filtered for analysis, they were removed, leading to an apparent decrease in Ca,  
292 Ba and Sr leaching. It will be necessary to perform further monolith leaching experiments to

293 examine the properties of the altered layer so that the origin of the fluctuations in these  
294 elements can be determined and set in the context of recent mechanistic studies of UK HLW  
295 and ILW glass performance [40-43].

## 296 **4 - Discussion**

297 Previous work has shown that cement may not have the capacity to effectively immobilise  
298 the diverse inventory of radioactive elements present in the PFR raffinate waste stream [44].  
299 Cementitious wastefoms could be subject to increased dissolution and release rates due to  
300 their inherent porosity and high internal surface area. The high solubility and potential for  
301 removal of many of the waste elements which sorb to the cement surface; especially Cs,  
302 which makes up over 60% of the radioactive inventory by activity, is of potential concern [2].  
303 These factors highlight the opportunity to vitrify PFR wastes to minimise radioisotope  
304 migration to the biosphere. Vitrification, using G73 barium silicate glass described in this  
305 investigation, is likely to offer significant improvements in long term wasteform performance  
306 over the current baseline.

307 The benefits of vitrification reach beyond the improvements in wasteform quality described  
308 and may also offer fiscal incentives, for example, by substantially reducing the waste volumes  
309 for storage and disposal. The current lifecycle waste management plan is to cement the PFR  
310 raffinate in 500 L drums, with a target waste loading of 0.305 m<sup>3</sup> per drum. With 212.1 m<sup>3</sup> of  
311 raffinate to process this would result in 397 m<sup>3</sup> of packaged waste for disposal (696 x 500 L  
312 drums with a displacement volume of 0.57 m<sup>3</sup> each) [2]. If vitrification, at 20 wt% loading was  
313 to be utilised, the volume of waste produced would be reduced to < 14.4 m<sup>3</sup> of glass.  
314 Conceivably, this volume of material could be readily processed in a small or modular plant,

315 utilising one of a variety of thermal treatment options for ILW being developed in the UK e.g.  
316 plasma vitrification, resistive heating melters or Hot-Isostatic Pressing [45].

317 Assuming packaging of vitrified PFR waste into 3 m<sup>3</sup> ILW boxes was preferable and 70% of the  
318 box capacity (2.57 m<sup>3</sup>) could be filled, each 3 m<sup>3</sup> box would hold 1.8 m<sup>3</sup> of vitrified product. In  
319 this scenario, the waste could be fully conditioned using just eight 3 m<sup>3</sup> boxes, producing a  
320 total waste volume for disposal of 28.6 m<sup>3</sup>. This treatment methodology, when compared  
321 with cementation, would reduce the waste disposal inventory by more than 90%, and, in  
322 principle, could be achieved, using in-container Joule heated melter technology. The heat  
323 generation, surface activity limits and containment limits for impact of this hypothetical G73-  
324 20 waste stream have been estimated to be within existing guidelines for a 3 m<sup>3</sup> ILW box<sup>1</sup>  
325 [46]. The substantial volume reduction achieved by the vitrification approach would enable  
326 transfer of the resulting waste packages to the Sellafield site for storage, potentially assisting  
327 earlier closure of the Dounreay site.

328 Deriving a lifetime waste management cost for these wastes intended for near surface  
329 storage has not been attempted here. However, it is believed the cost reductions associated  
330 with managing lower volumes of wastes in the rest of the NDA estate should be transferable  
331 to Scottish policy. It is important to note that the volume reduction and concentration of the  
332 waste associated with this vitrification step would not result in the re-classification of the  
333 waste as HLW. This is important as a reclassification to HLW would require consideration of  
334 heat dissipation in storage, introducing significant extra costs for disposal, as well as  
335 increasing the final volume required in a storage vault.

---

<sup>1</sup> Calculation based upon reported inventory of radioisotopes for this waste stream and accounting for the concentration of activity achieved by vitrification. This packaged waste will meet stated specifications imposed for a square corner 3 m<sup>3</sup> box.

336 The decreased risk to public health, superior quality of final wasteform, improved long term  
337 stability, smaller footprint on the Dounreay ILW stores and the reduced waste management  
338 cost, combine to provide a credible case for treatment of these wastes using vitrification over  
339 cementation.

## 340 **5 - Conclusion**

341 A vitreous wasteform for simulant PFR raffinate was developed at a range of waste loadings  
342 up to 20 wt%. **The product was a stable and homogeneous amorphous solid with no**  
343 **observable crystal formation.** All glasses performed comparably to vitrified waste  
344 compositions currently in use, both in the UK and internationally, for the immobilisation of  
345 HLW. The aqueous durability was superior to that of current UK HLW glasses under  
346 comparable experimental conditions. Therefore, the glasses investigated here could be  
347 considered a stable matrix for ILW under both geological disposal and near-surface storage  
348 scenarios. The mechanical properties of the wasteform also matched or exceeded those  
349 currently in use for HLW glasses, in both the UK and USA, and therefore, should be amenable  
350 to transport and storage in either 500 L HLW flasks or 3 m<sup>3</sup> ILW waste packages. Additionally,  
351 we demonstrated that undertaking immobilisation of PFR raffinate through thermal  
352 treatment methods may also result in a decrease in the anticipated volume of waste from  
353 397 m<sup>3</sup> to 28.6 m<sup>3</sup>, potentially resulting in significant lifetime waste management cost savings  
354 and a more robust option to support the Scottish policy for at near surface storage and site  
355 closure.

## 356 **Acknowledgements**

357 The authors would like to thank Paul Lythgoe and Alastair Bewsher (School of Earth Science,  
358 University of Manchester) for performing the XRF and ICP-AES measurements presented in

359 this work, Martina Klinkenberg and Jülich Forschungszentrum for access to the FEI SEM. This  
360 research was performed in part at the MIDAS Facility, at the University of Sheffield, which  
361 was established with support from the Department of Energy and Climate Change. We are  
362 grateful to EPSRC for sponsorship of this research under grants EP/G037140/1,  
363 EP/N017870/1, and EP/N017374/1.

## 364 **References**

- 365 [1] S.E. Jensen, P.L. Ølgaard, Description of the prototype fast reactor at Dounreay,  
366 NKS/RAK-2(95)TR-C 1, Rise National Laboratory, Roskilde, Denmark, NKS, 1996.  
367 [http://www.iaea.org/inis/collection/NCLCollectionStore/\\_Public/28/026/28026107.pdf](http://www.iaea.org/inis/collection/NCLCollectionStore/_Public/28/026/28026107.pdf)  
368 (accessed January 7, 2017).
- 369 [2] Nuclear Decommissioning Authority, Waste Stream 5B01 - PFR Raffinate, UK Radioactive  
370 Waste Inventory, (2014).
- 371 [3] K.F. Langley, B.A. Partridge, M. Wise, Immobilization of Fast Reactor First Cycle Raffinate,  
372 in: Proceedings of Waste Management - Tuscon AZ, 2003.  
373 <http://www.wmsym.org/archives/2003/pdfs/50.pdf> (accessed January 7, 2017).
- 374 [4] United Kingdom Atomic Energy Authority (UKAEA), Justification for Classifying PFR  
375 Raffinate as ILW, DSRPTC (2003) P11, (2003).
- 376 [5] United Kingdom Atomic Energy Authority (UKAEA), How To Deal with the Management  
377 of Prototype Fast Reactor (PFR) Raffinate, UKAEA/PP/P(2004)01, (2004).
- 378 [6] United Kingdom Atomic Energy Authority (UKAEA), Best Practicable Environmental  
379 Option Study For The Management of PFR Raffinate, D3900(04)P027, (2005).
- 380 [7] Nuclear Decommissioning Authority, Waste Stream 5B04 - MTR Raffinate, UK  
381 Radioactive Waste Inventory, (2014).
- 382 [8] Nuclear Decommissioning Authority, Waste Stream 5B05 - DFR Raffinate, UK Radioactive  
383 Waste Inventory, (2014).
- 384 [9] J.H. Sharp, J. Hill, N.B. Milestone, E.W. Miller, Cementitious Systems for Encapsulation of  
385 Intermediate Level Waste, in: Proceedings of ICEM '03: The 9th International Conference  
386 on Radioactive Waste Management and Environmental Remediation, Oxford, UK, 2003.
- 387 [10] F. P. Glasser, Mineralogical Aspects of Cement in Radioactive Waste Disposal,  
388 Mineralogical Magazine. 65 (2001) 621–633.
- 389 [11] N.B. Milestone, Y. Bai, C.H. Yang, X.C. Li, The Use of Activated Slags as Immobilisation  
390 Matrices for ILW, in: MRS Online Proceedings Library, 2008: p. 93.
- 391 [12] Committee on Radioactive Waste Management (CoRWM), Response to Scotland's Policy  
392 on Higher Activity Radioactive Waste: Consultation on an Implementation Strategy,  
393 CoRWM document .3220, (2015).
- 394 [13] Scottish Government, Consultation on an Implementation Strategy for Scotland's Policy  
395 on Higher Activity Radioactive Waste, (2015).

- 396 [14] E.R. Merz, D. Dyckerhoff, R. Odoj, Characterization of radioactive wastes incorporated in  
397 a cement matrix, in: Proceedings of International Conference on Radioactive Waste  
398 Management, 1986: pp. 396–401.
- 399 [15] H.J. Mockel, R.H. Koster, Gas Formation During the Gamma Radiolysis of Cemented Low-  
400 and Intermediate-Level Waste Products, NT. 59 (1982) 494–497.
- 401 [16] N.E. Bibler, Radiolytic gas production from concrete containing Savannah River Plant  
402 waste, Du Pont de Nemours (E.I.) and Co., 1978.  
403 [http://inis.iaea.org/Search/search.aspx?orig\\_q=RN:9389931](http://inis.iaea.org/Search/search.aspx?orig_q=RN:9389931) (accessed February 9,  
404 2017).
- 405 [17] C. A Utton, I. H. Godfrey, Review of stability of cemented grouted ion-exchange  
406 materials, sludges and flocs January, (2010).  
407 [https://rwm.nda.gov.uk/publication/review-of-stability-of-cemented-grouted-ion-](https://rwm.nda.gov.uk/publication/review-of-stability-of-cemented-grouted-ion-exchange-materials-sludges-and-flocs-january-2010/)  
408 [exchange-materials-sludges-and-flocs-january-2010/](https://rwm.nda.gov.uk/publication/review-of-stability-of-cemented-grouted-ion-exchange-materials-sludges-and-flocs-january-2010/) (accessed February 9, 2017).
- 409 [18] P.A. Bingham, N. C. Hyatt, R. J. Hand, C.R. Wilding, P.A. Bingham, N.C. Hyatt, R.J. Hand,  
410 C.R. Wilding, Glass Development for Vitrification of Wet Intermediate Level Waste  
411 (WILW) from Decommissioning of the Hinkley Point 'A' Site, MRS Online Proceedings  
412 Library, 1124 (2008) 1124-Q03-07., in: MRS Online Proceedings Library, 2008: pp. Q03-  
413 07.
- 414 [19] P.A. Bingham, N.C. Hyatt, R.J. Hand, Vitrification of UK intermediate level radioactive  
415 wastes arising from site decommissioning: property modelling and selection of  
416 candidate host glass compositions, Glass Technology – European Journal of Glass Science  
417 & Technology Part A, 53, 2012, 83-100.
- 418 [20] P.A. Bingham, N.C. Hyatt, R.J. Hand, S.D. Forder, Vitrification of UK intermediate level  
419 radioactive wastes arising from site decommissioning. Initial laboratory trials, Glass  
420 Technology – European Journal of Glass Science & Technology Part A, 54, 2013, 1-19.
- 421 [21] O.J. McGann, P.A. Bingham, R.J. Hand, A.S. Gandy, M. Kavcic, M. Zitnik, K. Bucar, R. Edge,  
422 N.C. Hyatt,., The Effects of  $\gamma$ -radiation on Model Vitreous Wasteforms Intended for the  
423 Disposal of Intermediate and High Level Radioactive Wastes in the United Kingdom,  
424 Journal of Nuclear Materials. 429 (2012) 353–367.
- 425 [22] C.P. Kaushik, R.K. Mishra, P. Sengupta, A. Kumar, D. Das, G.B. Kale, K. Raj, Barium  
426 borosilicate glass – a potential matrix for immobilization of sulfate bearing high-level  
427 radioactive liquid waste, Journal of Nuclear Materials. 358 (2006) 129–138.
- 428 [23] B. Brendebach, M.A. Denecke, G. Roth, S. Weisenburger, Sulfur incorporation in high level  
429 nuclear waste glass: A S K-edge XAFS investigation, J. Phys.: Conf. Ser. 190 (2009)  
430 012186.
- 431 [24] C.H. Oh, Hazardous and radioactive waste treatment technologies handbook, CRC Press,  
432 2001.
- 433 [25] C 1285-02 Standard Test Methods for Determining Chemical Durability of Nuclear,  
434 Hazardous, and Mixed Waste Glasses and Multiphase Glass Ceramics: The Product  
435 Consistency Test (PCT), ASTM International, (2008).
- 436 [26] A.J. Connelly, R.J. Hand, P.A. Bingham, N.C. Hyatt, Mechanical properties of nuclear  
437 waste glasses, Journal of Nuclear Materials. 408 (2011) 188–193.
- 438 [27] M. Asano, T. Kou, Y. Mizutani, Vaporization of Alkali Borosilicate Glasses, Journal of Non-  
439 Crystalline Solids. 112 (1989) 381–384.
- 440 [28] B.G. Parkinson, Influence of Composition on Structure and Caesium Volatilisation from  
441 Glasses for HLW Confinement, The University of Warwick, 2007.

- 442 [29] J. E. Shelby, *An Introduction to Glass Science and Technology*, 2nd ed., The Royal Society  
443 of Chemistry, Cambridge, 2005.
- 444 [30] R. Short, Phase Separation and Crystallisation in UK HLW Vitrified Products, *Procedia*  
445 *Materials Science*. 7 (2014) 93–100. doi:10.1016/j.mspro.2014.10.013.
- 446 [31] M.H. Langowski, J.G. Darab, P.A. Smith, Volatility literature of chlorine, iodine, cesium,  
447 strontium, technetium, and rhenium; technetium and rhenium volatility testing, Pacific  
448 Northwest Lab., 1996. [http://inis.iaea.org/Search/search.aspx?orig\\_q=RN:27054276](http://inis.iaea.org/Search/search.aspx?orig_q=RN:27054276)  
449 (accessed January 13, 2017).
- 450 [32] I.W. Donald, B.L Metcalfe, R.N.J. Taylor, The Immobilization of High Level Radioactive  
451 Wastes Using Ceramics and Glasses, *Journal of Materials Science*. 32 (1997) 5851–5887.
- 452 [33] H.U. Zwicky, B. Grambow, C. Magrabi, E.T. Aerne, Corrosion Behaviour of British Magnox  
453 Waste Glass in Pure Water, *MRS Online Proceedings Library*. 127 (1988) 127–129.
- 454 [34] L. Wang, *Advances in Transport Phenomena: 2009*, Springer Science & Business Media,  
455 2009.
- 456 [35] C. A. Utton, R. J. Hand, N. C. Hyatt, S. W. Swanton, S. J. Williams, Formation of alteration  
457 products during dissolution of vitrified ILW in a high-pH calcium-rich solution. *Journal of*  
458 *Nuclear Materials*, 4421, 33 – 45, 2013, *Journal of Nuclear Materials*. 4421 (2013) 33–  
459 45.
- 460 [36] S. Mercado-Depierre, F. Angeli, F. Frizon, S. Gin, Antagonistic effects of calcium on  
461 borosilicate glass alteration, *Journal of Nuclear Materials*. 441 (2013) 402–410.
- 462 [37] S. Gin, P. Jollivet, M. Fournier, C. Berthon, Z. Wang, A. Mirtoshkov, Z. Zhu, J. V. Ryan, The  
463 fate of silicon during glass corrosion under alkaline conditions: A mechanistic and kinetic  
464 study with the International Simple Glass, *Geochimica et Cosmochimica Acta*. 151 (2015)  
465 68–85.
- 466 [38] C.A. Utton, S.W. Swanton, J. Schofield, R.J. Hand, A. Clacher, N.C. Hyatt, Chemical  
467 durability of vitrified wastefoms: effects of pH and solution, *Mineralogical Magazine*, 76  
468 (2012), 2919-2930.
- 469 [39] C. L. Corkhill, N. J. Cassingham, P. G. Heath, N. C. Hyatt, Dissolution of UK high level waste  
470 glass under simulated hyperalkaline conditions of a co-located geological disposal  
471 facility, *International Journal of Applied Glass Science*. 4 (2013) 341–356.
- 472 [40] N. Cassingham, C.L. Corkhill, D.J. Backhouse, R.J. Hand, J.V. Ryan, J.D. Vienna, N.C. Hyatt,  
473 The initial dissolution rates of simulated UK Magnox-ThORP blend nuclear waste glass as  
474 a function of pH, temperature and waste loading, *Mineralogical Magazine*, 79, 2015,  
475 1529-1542.
- 476 [41] H. Zhang, C.L. Corkhill, P.G. Heath, R.J. Hand, M.C. Stennett, N.C. Hyatt, Effect of Zn- and  
477 Ca oxides on the structure and chemical durability of simulant alkali borosilicate glasses  
478 for immobilisation of UK high level wastes, *Journal of Nuclear Materials*, 462, 2015, 321-  
479 328.
- 480 [42] N.J. Cassingham, C.L. Corkhill, M.C. Stennett, R.J. Hand, Alteration layer formation of Ca-  
481 and Zn-oxide bearing alkali borosilicate glasses for immobilisation of UK high level waste:  
482 A vapour hydration study, *Journal of Nuclear Materials*, 479, 2016, 639-646.
- 483 [43] N.C. Hyatt, R.R. Schwarz, P.A. Bingham, M.C. Stennett, M. C. C.L. Corkhill, P.G. Heath, R.J.  
484 Hand, M. James, A. Pearson, S. Morgan, Thermal treatment of simulant plutonium  
485 contaminated materials from the Sellafield site by vitrification in a blast-furnace slag,  
486 *Journal of Nuclear Materials*, 444, 2014, 186-199.
- 487 [44] M. Atkins, F. P. Glasser, Application of Portland Cement-Based Materials to Radioactive  
488 Waste Immobilization, *Waste Management*. 12 (1992) 105–131.

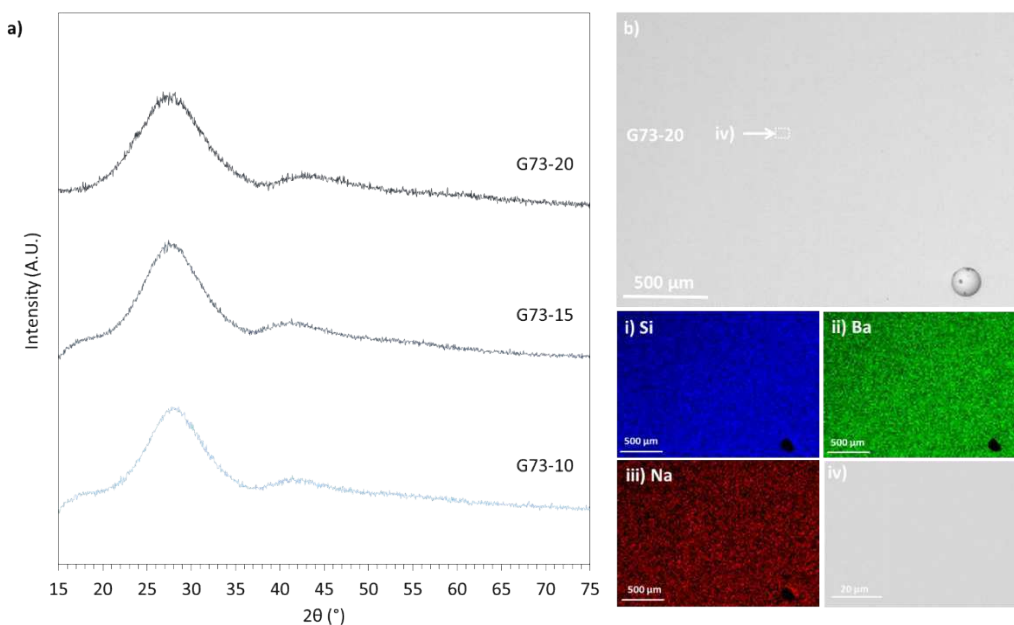
489 [45] N.C. Hyatt, M. James, Thermal treatment of ILW, Nuclear Engineering International. 58  
490 (2013) 10–13.

491 [46] G. Steele, Areva Risk Management Consulting, Contents Activity for the Square Corner 3  
492 m<sup>3</sup> Box Waste Package Transported in an SWTC-285 Transport Container, NDA.RWMD.  
493 R07-023(C) J6214.23, (2009).

494

495

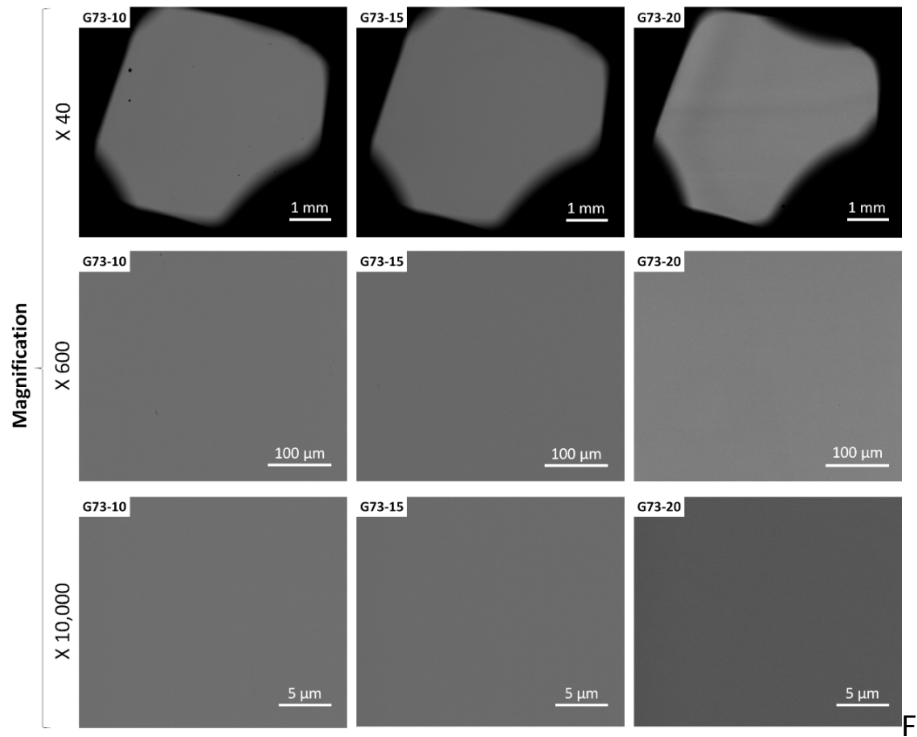
496 **Figures**



497

498 Figure 1 - a) Powder XRD patterns of G73 PFR raffinate loaded glasses, displaying diffuse scattering characteristic of  
499 amorphous material and b) SEM-BSE image displaying homogeneity of G73-20 glass matrix, set above i) - iii) SEM-EDX  
500 maps of key elements for b) and iv) a higher resolution BSE-SEM of G73-20 glass matrix identified in b) which taken  
501 illustrates the absence of crystalline materials in the final waste product.

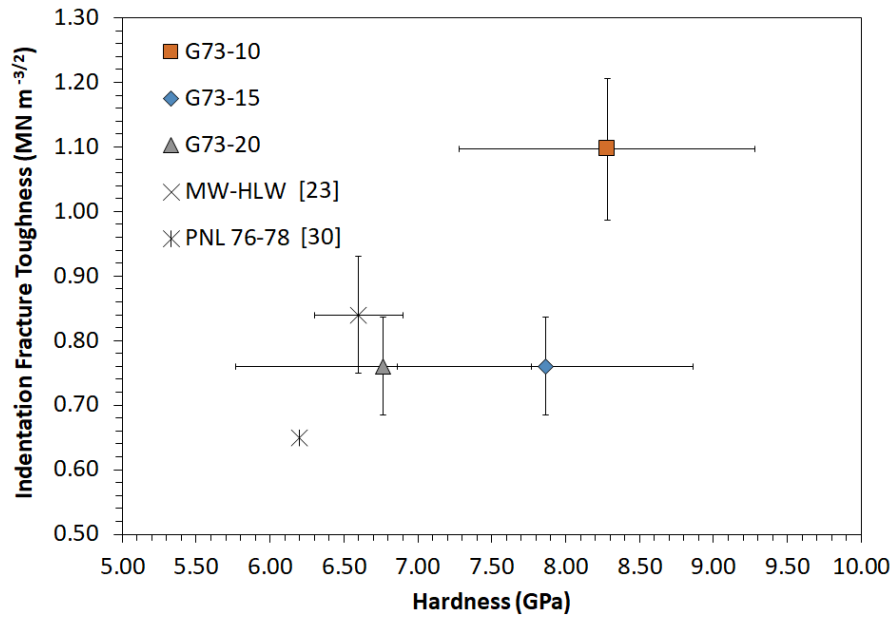
502



503

504 Figure 2 - SEM-BSE images of the three waste loaded glasses G73-10, G73-15 and G73-20 at various magnifications. The  
 505 lack of image contrast suggests chemical homogeneity within the sample.

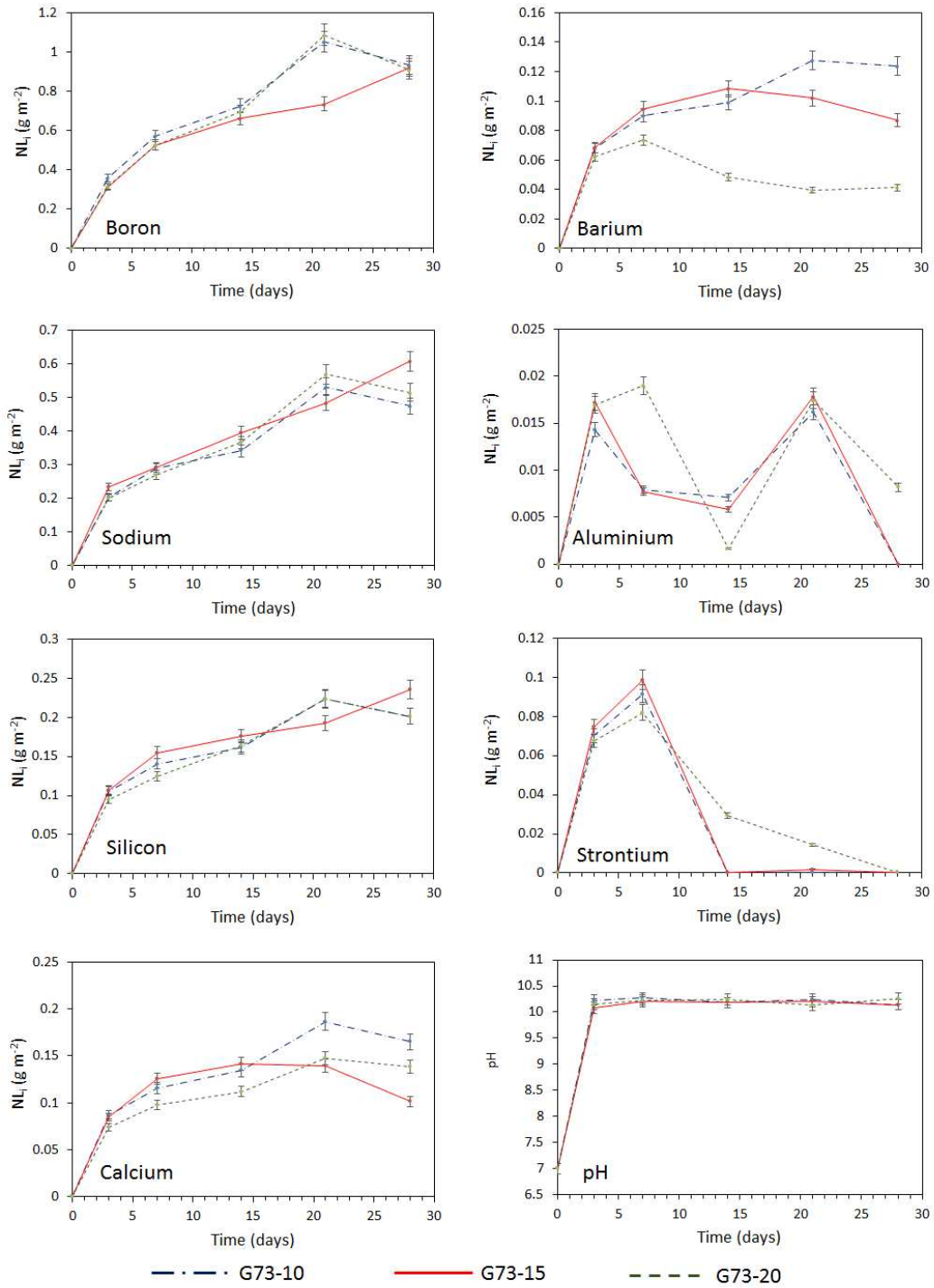
506



507

508 **Figure 3 - Indentation fracture toughness and hardness values of G73 PFR raffinate waste loaded glasses obtained using**  
 509 **the Vickers indentation methodology, with comparison to waste glasses currently used for HLW immobilisation [23,30].**  
 510 **Errors correspond to 3 x the measured standard deviation.**

511



512

513 Figure 4 - Graphs displaying the normalised elemental mass loss with varying levels of PFR raffinate loading from PCT  
 514 experiments at 90°C in 18.2 MΩ water with a SA/V of 1499 m<sup>-1</sup>-1525 m<sup>-1</sup> (dependant on glass density).

515

516 **Tables**

Included in Simulant (surrogate element used)		Excluded from Simulant	
<i>Element</i>	<i>ppm</i>	<i>Element</i>	<i>ppm</i>
<i>Na</i>	9,711	<i>Rh</i>	15
<i>Cu</i>	8,725	<i>Cm</i>	4
<i>Fe</i>	3,837	<i>Nb</i>	3.5
<i>Zn</i>	3,566	<i>Dy</i>	2.4
<i>Cd</i>	2,540	<i>Ag</i>	<1.3
<i>S</i>	1,351	<i>As</i>	<13
<i>Ni</i>	1,277	<i>Co</i>	<0.4
<i>Cr</i>	669	<i>Ge</i>	<1.3
<i>Cs</i>	509	<i>Hg</i>	<0.3
<i>Nd</i>	462	<i>Ho</i>	<1.3
<i>Am (Sm)</i>	405	<i>In</i>	<4
<i>Al</i>	350	<i>Np</i>	<13
<i>Ce</i>	304	<i>P</i>	<2.7
<i>U (Ce)</i>	168	<i>Pb</i>	<1.1
<i>La</i>	163	<i>Rb</i>	<1.3
<i>Pr</i>	158	<i>Sb</i>	<1.3
<i>Mo</i>	154	<i>Se</i>	<1.3
<i>Pd</i>	150	<i>Sn</i>	<0.3
<i>Ca</i>	138	<i>Tc</i>	<1.3
<i>Sm</i>	123	<i>Eu</i>	15
<i>Y</i>	112	<i>Gd</i>	15
<i>Te</i>	74	<i>Pd</i>	150
<i>Sr</i>	60		
<i>Mn</i>	45		
<i>Ru</i>	60		
<i>Ba</i>	39		
<i>Ti</i>	36		
<b>Total</b>	<b>35,186</b>	<b>Total</b>	<b>205</b>

517 Table 1 - Average composition of PFR raffinate as characterised in [6]. (Brackets) indicate where the use of an appropriate  
518 inactive simulant was applied. The right-hand columns identifies elements excluded from the simulant based on both low  
519 concentrations in the raffinate and on an economic basis.

520  
521  
522

Table 2 - Compositions of base glass, simulant calcined PFR raffinate and glasses produced. Compositions of glasses provided both as batched and as measured by XRF (boron analysis via dissolution in HF and ICP-AES). \*Note glasses were batched to 100 wt%; discrepancies reported result from rounding to 2 d.p.

Component (wt%)	G73-00 Base Glass	PFR Calcine	G73-10		G73-15		G73-20	
			Batch	Meas.	Batch	Meas.	Batch	Meas.
SiO <sub>2</sub>	42.0	0.00	37.80	34.29	35.70	33.4	33.60	32.58
BaO	42.0	0.09	37.81	41.21	35.71	41.61	33.62	38.61
Fe <sub>2</sub> O <sub>3</sub>	6.00	11.68	6.57	7.88	6.85	7.78	7.14	7.56
CaO	5.00	0.41	4.54	4.55	4.31	4.54	4.08	4.40
Na <sub>2</sub> O	2.50	27.88	5.04	1.64	6.31	2.38	7.58	3.30
CuO	0	26.26	2.63	2.83	3.94	3.98	5.25	5.05
B <sub>2</sub> O <sub>3</sub>	2.00	0.00	1.80	0.46	1.70	0.56	1.60	0.46
ZnO	0	9.45	0.95	1.08	1.42	1.55	1.89	1.93
CdO	0	6.18	0.62	0.74	0.93	1.05	1.24	1.35
SO <sub>3</sub>	0	7.18	0.72	0.72	1.08	0.79	1.44	0.86
Al <sub>2</sub> O <sub>3</sub>	0.50	1.41	0.59	0.86	0.64	0.85	0.68	1.2
NiO	0	3.46	0.35	0.55	0.52	0.71	0.69	0.86
Cr <sub>2</sub> O <sub>3</sub>	0	2.08	0.21	0.48	0.31	0.56	0.42	0.66
Cs <sub>2</sub> O	0	1.15	0.12	0.36	0.17	0.42	0.23	0.52
Nd <sub>2</sub> O <sub>3</sub>	0	1.15	0.12	0.15	0.17	0.00	0.23	0.23
Sm <sub>2</sub> O <sub>3</sub>	0	0.30	0.03	0.10	0.05	0.14	0.06	0.19
CeO <sub>2</sub>	0	0.97	0.10	0.05	0.15	0.10	0.19	0.12
MoO <sub>3</sub>	0	0.49	0.05	0.06	0.07	0.08	0.10	0.09
Y <sub>2</sub> O <sub>3</sub>	0	0.30	0.03	0.03	0.05	0.05	0.06	0.06
La <sub>2</sub> O <sub>3</sub>	0	0.04	0.00	0.03	0.01	0.00	0.01	0.04
Pr <sub>6</sub> O <sub>11</sub>	0	0.04	0.00	0.04	0.01	0.06	0.01	0.09
RuO <sub>2</sub>	0	0.17	0.02	0.00	0.03	0.00	0.03	0.00
SrO	0	0.15	0.02	0.6	0.02	0.12	0.03	0.07
TeO <sub>2</sub>	0	0.20	0.02	0.00	0.03	0.00	0.04	0.00
TiO <sub>2</sub>	0	0.13	0.01	0.00	0.02	0.00	0.03	0.00
Mn <sub>2</sub> O <sub>3</sub>	0	0.14	0.01	0.08	0.02	0.08	0.03	0.09
	100	-	100.13	98.795	100.20	100.81	100.26	100.32

524

Glass Property	Sample ID		
	G73-10	G73-15	G73-20
Density (g cm <sup>-3</sup> )	3.512 ± 0.002	3.572 ± 0.002	3.574 ± 0.003
Glass Transition Temperature (°C)	470 ± 10	483 ± 10	484 ± 10
Liquidus Temperature (°C)	1045 ± 10	1075 ± 10	1020 ± 10

525 [Table 3 - Properties of glass wastefoms produced at varying PFR raffinate waste loadings including the density, liquidus](#)  
526 [temperature \(measured in mullite crucibles - see main text for the implication of this\) and glass transition temperature.](#)

527

NR <sub>i</sub> (g m <sup>-2</sup> day <sup>-1</sup> )	Glass Composition		
	G73-10	G73-15	G73-20
B	3.33 x 10 <sup>-2</sup>	3.28 x 10 <sup>-2</sup>	3.24 x 10 <sup>-2</sup>
Na	1.69 x 10 <sup>-2</sup>	2.17 x 10 <sup>-2</sup>	1.84 x 10 <sup>-2</sup>
Si	7.18 x 10 <sup>-3</sup>	8.40 x 10 <sup>-3</sup>	7.19 x 10 <sup>-3</sup>
Ca	5.89 x 10 <sup>-3</sup>	3.62 x 10 <sup>-3</sup>	4.95 x 10 <sup>-3</sup>
Mo	4.44 x 10 <sup>-3</sup>	4.78 x 10 <sup>-3</sup>	6.38 x 10 <sup>-3</sup>
Ba	4.43 x 10 <sup>-3</sup>	3.10 x 10 <sup>-3</sup>	1.47 x 10 <sup>-3</sup>
Cr	3.48 x 10 <sup>-4</sup>	1.64 x 10 <sup>-4</sup>	2.30 x 10 <sup>-4</sup>
Cu	4.93 x 10 <sup>-6</sup>	1.45 x 10 <sup>-6</sup>	0.00
Al	0.00	0.00	2.91 x 10 <sup>-4</sup>
Fe	0.00	0.00	0.00
Ni	0.00	0.00	0.00
Sr	0.00	0.00	0.00
Zn	0.00	0.00	0.00

528 [Table 4 - Normalised elemental loss rates for the three waste PFR waste loaded glasses measured after 28 days. Data is](#)  
529 [from PCT experiments of the wasteforms at 90 °C in 18.2 MΩ water.](#)

530

Glass Composition	NL <sub>i</sub> after 28 days (g m <sup>-2</sup> )		NR <sub>i</sub> after 28 days (g m <sup>2</sup> day <sup>-1</sup> )		SA/V (m <sup>-1</sup> )	pH (25 °C)
	NL <sub>B</sub>	NL <sub>Si</sub>	NR <sub>B</sub>	NR <sub>Si</sub>		
G73-20	0.9076	0.2012	0.0324	0.0072	1499	10.26
SON68 [40]	0.4886	0.1559	0.0175	0.0055	2135	9.4
MW25 [31]	8.89	0.538	0.32	0.020	1200	-

531 Table 5 - Comparison of network dissolution limiting normalised elemental mass losses and normalised elemental  
532 dissolution rates between SON68 glass, British Magnox waste HLW glass and G73-15 waste loaded glasses tested, under  
533 PCT conditions at 90 °C in 18.2 MΩ water.

534

1

## 2 **Immobilisation of Prototype Fast Reactor Raffinate using Barium**

### 3 **Silicate ILW Glasses**

4 Paul G. Heath, Claire L. Corkhill, Martin C. Stennett, Russell J. Hand, Kieran M. Whales, Neil C.  
5 Hyatt

6 Immobilisation Science Laboratory, Sir Robert Hadfield Building, Mappin Street, The  
7 University of Sheffield, Sheffield, S1 3JD, United Kingdom

#### 8 **Abstract**

9 The vitrification of Dounreay Prototype Fast Reactor Raffinate (PFR) in a barium borosilicate  
10 glass matrix was investigated, with the aim of understanding process feasibility and the  
11 potential benefits over the current baseline of cement encapsulation. Laboratory scale glass  
12 melts demonstrated the production of homogeneous glasses incorporating at least 20 wt%  
13 simulant PFR waste (on an oxides basis), with no detectable crystalline accessory phases. The  
14 hardness and indentation fracture toughness of the simulant PFR waste glasses were  
15 determined to be comparable to those of current UK high level waste glass formulations. The  
16 normalised dissolution rate of boron from the simulant PFR glasses was determined to be  $3 \times$   
17  $10^{-2} \text{ g m}^{-2} \text{ d}^{-1}$ , in  $18.2 \text{ M}\Omega$  water at  $90^\circ\text{C}$  and surface area / volume ratio of  $1500 \text{ m}^{-1}$ ; only a  
18 factor of two greater than the French SON-68 simulant high level waste glass, under  
19 comparable conditions. Consequently, the simulant PFR waste glasses are considered to  
20 show considerable promise for meeting envisaged waste acceptance criteria for geological  
21 disposal. Overall, the superior stability of vitrified PFR wasteforms could enhance the safety

- 22 case for long term near surface storage of radioactive wastes, mandated by current Scottish
- 23 Government policy.
- 24 Keywords: Amorphous Materials, Waste Immobilisation, Mechanical properties.

## 25 Introduction

26 The Prototype Fast Reactor (PFR) was the UK's second fast reactor and operated between  
27 1974 and 1994, utilising a high plutonium content mixed oxide fuel (MOx) with a molten  
28 sodium coolant [1]. Spent fuel from the PFR was reprocessed on the Dounreay site by  
29 dissolution in nitric acid to recover the reusable fissile material. This process yielded  
30 approximately 200 m<sup>3</sup> of an aqueous radioactive liquor, known as PFR raffinate [2]. The PFR  
31 raffinate contains the majority of the radioactive material and fission products produced  
32 during the operation of the PFR reactor and on the Dounreay site as a whole [3]. Since the  
33 reprocessing of PFR fuel was completed in 1996, the waste raffinate has been stored in  
34 underground tanks on the Dounreay site. Having spent a decade in storage, PFR raffinate was  
35 reclassified as Intermediate Level Waste in 2004, ostensibly due to its low heat output [4].

36 The conditioning of PFR raffinate into a passively safe, wasteform is identified as a priority in  
37 the Dounreay Site Restoration Plan [5]. A best practical environmental option assessment,  
38 undertaken by the UKAEA, proposed neutralisation and cementation of the raffinate as the  
39 reference waste management strategy [6]. For this waste treatment option to be  
40 implemented, a new facility (to be known as D3900) is required, the construction of which is  
41 yet to begin at the time of writing.

42 Although laboratory studies have demonstrated that cement-encapsulated *inactive* raffinate  
43 has physical properties comparable to those of other cemented ILW streams (e.g. viscosity,  
44 initial setting time, bleed water), PFR raffinate has a specific activity 20 times greater than  
45 other encapsulated ILW streams [2,3,7,8]. The high concentration of <sup>137</sup>Cs in PFR raffinates,  
46 the porous nature and poor immobilisation of Cs observed in cementitious systems, may limit  
47 the ability of cement to retain the radioactive inventory of PFR [2,9-11]. It is not yet certain  
48 that environmental release rates from a cemented PFR raffinate wasteform will be within

49 permitted limits over the relevant lifetime of the wastefrom, particularly given the policy of  
50 the Scottish Government for long term near-surface storage at a coastal location, as in the  
51 case of Dounreay [12,13].

52 An issue that may be even more significant to safe interim storage is the high specific activity  
53 of the wastes and their significant alpha emitting component ( $\beta/\gamma = 346 \text{ TBq m}^{-3}$ ,  $\alpha = 3.21$   
54  $\text{TBq m}^{-3}$ ) [2]. It is known that the radiolysis of cementitious water will produce  $\text{H}_2$ , while the  
55 presence of significant nitrate concentrations in the waste ( $300\text{-}500 \text{ g l}^{-1}$ ) and alpha activity  
56 will also result in the formation of  $\text{O}_2$  and  $\text{NO}_x$  [14–17]. These combined factors will increase  
57 the rate of gas generation when compared to existing UK ILW waste packages. As a result,  
58 these reactions could be expected to introduce significant complexities to the long-term  
59 management of cemented PFR raffinate waste packages through the need to monitor, vent  
60 and dissipate gases from the waste packages.

61 It should be noted that the near-surface storage policy was introduced after the strategic  
62 decision to encapsulate PFR raffinates in a cement wastefrom. In its response to the Scottish  
63 Government consultation on higher activity wastes, the Committee on Radioactive Waste  
64 Management (CoRWM) highlighted that certain wastes from the Dounreay site were “*never*  
65 *likely to be suitable for near surface disposal and therefore greater efforts need to be made in*  
66 *the interest of safety, security and intergenerational equity to find a permanent solution for*  
67 *this waste*” [12].

68 The current investigation aims to demonstrate, in principle, an alternative processing option  
69 for PFR raffinate, which could enhance the safety case for long term near-surface storage and  
70 address the concerns of CoRWM. A derivative of the barium borosilicate glass, G73, previously  
71 investigated as a matrix for the immobilisation of UK ILWs arising at Magnox decommissioning  
72 sites [18-21], is here investigated as a disposal matrix for PFR raffinate, the composition of

73 which incorporates ca. 7 wt% SO<sub>3</sub>. Barium borosilicate glasses, such as G73, are reported to  
74 have a high aqueous durability and the presence of Ba is known to increase the solubility of  
75 sulphate species, which inhibits the formation of water soluble “yellow phase” salts [18-23].  
76 We present an analysis of the composition, amorphous nature, aqueous durability, thermal  
77 behaviour and mechanical properties of vitrified PFR raffinate with waste loadings of 10 wt%,  
78 15 wt% and 20 wt% (oxide basis), in a barium borosilicate glass. The results are discussed with  
79 reference to the potential benefits of PFR raffinate vitrification compared to cementation.

## 80 **2 - Materials and Experimental**

### 81 **2.1 - Materials**

#### 82 **2.1.1 Raffinate Simulant**

83 The inactive surrogate for PFR raffinate was formulated on the assumption that the waste  
84 would be treated using an evaporation or calcination step to produce a solid calcine prior to  
85 vitrification. The composition was thus formulated using the data available on the average  
86 composition of four PFR tanks at the Dounreay site [6]. The chemical composition of model  
87 PFR raffinate is provided in Table 1. The solids content of the raffinate calcine was calculated  
88 based on the reported elemental values in the raffinate (ppm) and then converted to their  
89 oxide form, which is reported in Table 2.

90 Some variations in the elemental composition were necessary when batching the simulant.  
91 For example, for reasons of practicality, any elements with concentrations < 15 ppm were  
92 excluded (Ag, As, Cm, Dy, Eu, Gd, Ge, Hg, Ho, In, Nb, Np, P, Pb, Pd, Rb, Rh, Sb, Se, Sn and Tc).  
93 One exception was Pd, which was present at a concentration of ~150 ppm in the waste

94 stream. This was excluded on grounds of cost, for this preliminary study, and its known  
95 propensity to exist as an insoluble noble metal in glass melts [24].

96 The omission of the elements noted above accounted for < 2.8 wt% of the mass of the total  
97 waste stream. Radioactive elements with concentrations > 15 ppm were substituted by  
98 relevant concentrations of inactive surrogates (Ce for U and Sm for Am).

### 99 **2.1.2 Glass Preparation**

100 Three glasses were synthesised and characterised in this study. These glasses were based on  
101 a derivative of the G73 barium-silicate base glass composition (referred to here as G73, for  
102 simplicity), which was previously developed [18-21], with PFR raffinate simulant incorporated  
103 at 10 wt%, 15 wt% and 20 wt% waste loading. These glasses are identified as G73-10, G73-15  
104 and G73-20, respectively. The base glass composition, presented in Table 2 for reference, is  
105 identified as G73-00.

106 Glasses were produced from batch chemicals to provide 250 g of glass. The components of  
107 the raffinate simulant were batched in either their oxide or carbonate forms according to  
108 their molar proportions to obtain the specified waste loading. The following analytical grade  
109 chemicals were used for batching; Al(OH)<sub>3</sub>, Na<sub>2</sub>B<sub>4</sub>O<sub>7</sub>·10H<sub>2</sub>O, BaCO<sub>3</sub>, CaCO<sub>3</sub>, CdO, CeO<sub>2</sub>,  
110 Cr(NO<sub>3</sub>)<sub>3</sub>·9H<sub>2</sub>O, Cs<sub>2</sub>CO<sub>3</sub>, CuO, Fe<sub>2</sub>O<sub>3</sub>, La<sub>2</sub>O<sub>3</sub>, Mn<sub>2</sub>O<sub>3</sub>, MoO<sub>3</sub>, Na<sub>2</sub>CO<sub>3</sub>, Nd<sub>2</sub>O<sub>3</sub>, NiCO<sub>3</sub>, Pr<sub>6</sub>O<sub>11</sub>, RuO<sub>2</sub>,  
111 Na<sub>2</sub>SO<sub>4</sub>, SiO<sub>2</sub>, Sm<sub>2</sub>O<sub>3</sub>, SrCO<sub>3</sub>, TeO<sub>2</sub>, TiO<sub>2</sub>, Y<sub>2</sub>O<sub>3</sub> and ZnO. The batched powders were heated in  
112 mullite crucibles with stirring to 1200 °C at 10 °C min<sup>-1</sup> and held at temperature for 3 hours.  
113 The glasses were poured into blocks and annealed at 500 °C for one hour before cooling to  
114 25 °C at 1 °C min<sup>-1</sup>. Glass monoliths were prepared for SEM-EDX, Vickers hardness testing and  
115 fracture toughness testing to a 0.25 µm finish by successive grinding and polishing with SiC  
116 grit papers and diamond pastes. Powder samples were prepared using a hardened steel ring

117 and puck mill. The sub-75  $\mu\text{m}$  size fraction was collected for use in XRD and XRF analysis and  
118 the 75-150  $\mu\text{m}$  size fraction was collected for use in aqueous durability experiments and  
119 prepared according to ASTM standard C 1285 – 02 [25].

## 120 **2.2 - Characterisation**

### 121 **Glass Characterisation**

122 X-ray Fluorescence (XRF) analysis was performed using a Phillips PW2404 XRF Axios  
123 instrument to obtain compositional data.  $\text{B}_2\text{O}_3$  content was determined by dissolution of glass  
124 powder in HF followed by analysis of leachate using a Perkin-Elmer Optima 5300 dual view  
125 Inductively Coupled Plasma Atomic Emission Spectroscopy (ICP-AES). The density of the glass  
126 wastefoms was measured using a  $< 75 \mu\text{m}$  powder, using an AccuPyc 1340 II helium  
127 pycnometer with the following analysis regime; 200 purges of the chamber followed by 50  
128 cycles using an equilibration rate of  $35 \text{ Pa min}^{-1}$  at  $25 \text{ }^\circ\text{C}$  in a  $1 \text{ cm}^3$  chamber and a fill pressure  
129 of 86.2 KPa. Scanning Electron Microscopy was performed using a JEOL JSM 6400 SEM with  
130 an accelerating voltage of 20 kV and a working distance of 15 mm. Concurrent Energy  
131 Dispersive Spectroscopy was acquired (INCA, Oxford Instruments). Additionally, an FEI  
132 Quanta 200 F SEM was utilised for high resolution imaging, using an accelerating voltage of  
133 30 kV and working distance of 10 mm. Concurrent Energy Dispersive X-ray analysis was  
134 performed (Genesis EDX).

### 135 **Thermal and mechanical properties**

136 The glass liquidus temperature for each sample was measured by placing a 20 cm long mullite  
137 boat, filled with sub-75  $\mu\text{m}$  glass powder, into a tube furnace. The samples were left to  
138 equilibrate at  $1200 \text{ }^\circ\text{C}$  for 24 hours and the temperature gradient along the length of the boat  
139 at 5 mm intervals was measured using a retractable thermocouple. The boats were removed

140 and rapidly quenched in air. The point of crystallisation was measurable to within 1 mm by  
141 optical examination of the crucibles and this was then correlated with the associated  
142 temperature to estimate the liquidus temperature. Alterations in chemical composition  
143 resulting from crucible corrosion were not accounted for, nor were the phases produced  
144 analysed. As the purpose of this test was to check if the point of crystallisation was below  
145 1100 °C, and the contaminants from crucible corrosion are likely to lower this value, the  
146 results presented are considered useful in this context.

147 The Vickers hardness indentation method was used to determine both hardness ( $H_v$ ) and the  
148 indentation fracture toughness ( $K_C$ ) following the procedure described by Connelly et al. [26].  
149 Indentation was performed on a Mitutayo HM-101. Sixty indents were made at each of three  
150 indentation loadings; 0.98 N, 1.96 N and 2.94 N (twenty indents at each force per sample,  
151 error  $\pm 0.02$  N). The load was held for 20 seconds. Samples were left for 24 hours prior to  
152 analysis using optical microscopy. The Vickers hardness ( $H_v$ ) in Pa and the Fracture Toughness  
153 ( $K_C$ ) was calculated using Equations 1 and 2 respectively:

$$154 \quad H_v = \frac{1.854P}{(2a)^2} \quad \text{Equation 1}$$

$$155 \quad K_C = \frac{0.0824P}{c^{3/2}} \quad \text{Equation 2}$$

156 where  $P$  is the applied load (N),  $a$  is the half length of the indent diagonal (m) and  $c$  is the  
157 median/radial crack length (m). The results quoted are those obtained from the 1.96 N  
158 loading due to the higher number of acceptable indentations (a minimum of fifteen per  
159 sample).

160 **Aqueous durability assessment**

161 Aqueous durability assessment was performed according to ASTM standard C 1285 - 02  
162 (Product Consistency Test - PCT) utilising a 75 µm - 150 µm size fraction in 18.2 MΩ H<sub>2</sub>O at  
163 90°C with a SA/V between 1499 m<sup>-1</sup> and 1525 m<sup>-1</sup> dependent on glass density, as provided in  
164 Table 3 [25]. Experiments were performed in triplicate with duplicate blanks, sampling at 3,  
165 7, 14, 21 and 28 days. Samples were filtered using a 0.45 µm PTFE filter and leachate analysis  
166 was performed using ICP-AES.

167 The normalised elemental mass loss (NL<sub>*i*</sub>) and normalised elemental dissolution rates (NR<sub>*i*</sub>)  
168 were calculated according to Equations 3 and 4, respectively; using the analysed glass  
169 compositions.

170 
$$NL_i = \frac{C_i}{f_i \times \frac{SA}{V}} \quad \text{Equation 3}$$

171 
$$NR_i = \frac{C_i}{f_i \times \frac{SA}{V} \times t} \quad \text{Equation 4}$$

172 where NL<sub>*i*</sub> is the normalised elemental mass loss of element *i* (g m<sup>-2</sup>), C<sub>*i*</sub> is the averaged, blank  
173 corrected concentration of element *i* in solution (g m<sup>-3</sup>), f<sub>*i*</sub> is the fraction of element *i* in the  
174 unleached glass, SA/V is the ratio of glass surface area to the volume of water (m<sup>-1</sup>), NR<sub>*i*</sub> is the  
175 normalised elemental loss rate and t is time in days.

176 Geochemical modelling of the solution leachate was performed using the PhreeqC  
177 geochemical modelling code (v3-12-8538, provided by the United States Geological Survey)  
178 to identify solution saturation species, using the Lawrence Livermore National Laboratory  
179 (LLNL) thermodynamic database.

## 180 **3 - Results**

### 181 **3.1 - Glass Formation and Composition**

182 It can be stated with confidence that the three simulant PFR waste loaded G73 glasses exist  
183 within a stable glass forming region of the phase diagram up to a 20 wt% loading. The glasses  
184 formed readily and poured from the melt at 1200 °C, with no evidence of un-dissolved batch.  
185 However, a small degree of corrosion was evident inside the crucible, which is responsible for  
186 the elevated concentrations of alumina in the final composition. The composition of the three  
187 glasses was analysed using XRF and ICP-AES; data are shown in Table 2, which compares the  
188 final composition with the nominal batched compositions.

189 Overall, it can be seen from Table 2 that the batched and analysed compositions are in  
190 reasonable agreement for major and minor oxides, although with some notable exceptions.  
191 Na<sub>2</sub>O, B<sub>2</sub>O<sub>3</sub>, and SO<sub>3</sub>, are, in general, analysed as lower than the batched composition, due to  
192 volatilisation from the melts during high temperature processing. SiO<sub>2</sub> and BaO are,  
193 respectively, systematically higher and lower in the analysed glass compositions compared to  
194 the batched. The complexity of the glass composition made deconvolution of overlapping X-  
195 ray emission lines, from multiple elements, challenging and may be responsible for this  
196 systematic discrepancy. The loss of such volatile components from the melts does not pose  
197 a challenge to the off-gas system of existing HLW melter systems and, therefore, is not  
198 expected to be problematic for full scale deployment. In addition, it should be noted that the  
199 lower surface area to volume ratio, and presence of a cold cap, in full scale melter systems  
200 will reduce volatilisation considerably, with respect to laboratory scale melts.

201 Analysis of the vitrified products by X-ray diffraction showed only diffuse scattering (Figure 1)  
202 characteristic of an amorphous material, with no evidence of phase separation or detectable

203 crystallisation. The lack of contrast in both the SEM-BSE imaging and SEM-EDX mapping  
204 analysis, displayed in Figure 1b and Figure 2, is indicative of a chemically homogeneous glass  
205 on a micron scale. Each glass showed similar characteristics. There was no evidence from XRD  
206 or SEM-EDX analysis of distinct segregated sulphate phases.

207 Crystallisation in radioactive waste glasses, when produced from the melt, is undesirable for  
208 several reasons, including: the possibility for the precipitation of soluble radionuclide  
209 containing phases; the potential for decreased aqueous durability of the matrix, due to the  
210 removal of refractory components; and the potential for swelling of crystal phases as a result  
211 of damage from self-irradiation. The absence of significant crystallisation and minimal  
212 evidence of crucible corrosion indicate that a high-quality glass wasteform was obtained that  
213 should be both stable and amenable to the processing of PFR wastes.

### 214 **3.2 - Thermal Properties**

215 Table 3 shows the density, glass transition temperature and measured liquidus temperature  
216 of the simulant PFR glasses. The values obtained for the  $T_g$  are comparable, within error, for  
217 the three waste-loadings and correspond well with the transition temperature previously  
218 reported for the same base glass loaded with organic exchange resins [18-21].

219 The liquidus temperatures of the glasses were all below 1100 °C, and no correlation with  
220 increasing waste loading was observed. Glass compositions with a liquidus temperature  
221 below 1100 °C are thought to be beneficial for nuclear waste vitrification as the lower  
222 temperatures minimise volatile losses of radioactive components during melting [27-29].  
223 Although not essential for all melter operations or wasteform acceptance criteria, the  
224 absence of crystalline products indicates that the wasteforms will be amenable to commercial

225 application; due to the associated simplification of wastefrom qualification, improved  
226 efficiency of melter operation and predictability of process control [30]

227 As the glasses produced in this study have been shown to retain their Cs inventory after  
228 processing at 1200 °C, the retention of Cs should be expected to be retained in full scale melts  
229 given the smaller melt surface area to volume ratio and possibility of operating with a cold  
230 cap [31].

### 231 **3.3 - Mechanical Testing**

232 The Vickers hardness and indentation fracture toughness of the PFR simulant glasses are  
233 plotted in Figure 3. The fracture toughness of the glass relates to the energy required to form  
234 a new surface and is relevant to qualifying the suitability of radioactive waste packages for  
235 transport, e.g. in estimating the likelihood of respirable fines formation in accident scenario  
236 [32].

237 The lowest waste loaded glass, G73-10, had the highest indentation fracture toughness and  
238 the hardness value of the glasses tested. G73-15 and G73-20 glasses gave lower values and  
239 were equivalent within measurable precision. All compositions were comparable or superior  
240 to existing HLW glass compositions (e.g. UK MW glass and US PNL 76-78 glass, Fig. 3) for  
241 indentation fracture toughness and were comparable, or superior, in terms of Vickers  
242 hardness [26,32].

243 Although no specification for fracture toughness currently exists for UK vitreous waste  
244 packages, the results imply that, as the G73 based glasses are comparable to current  
245 wastefroms, they are likely to be compliant with storage in existing (HLW) canisters.  
246 Furthermore, the mechanical properties suggest that packaging in larger 3 m<sup>3</sup> boxes may also

247 be possible, although in this case analysis of thermally induced cracking/stresses during  
248 processing requires investigation.

### 249 **3.4 - Aqueous Durability**

250 The short-term chemical durability of the simulant raffinate glasses was investigated using  
251 the PCT methodology [25]. Figure 4 shows the normalised mass loss of elements that were  
252 detectable by ICP-AES in concentrations higher than those measured in the blank solutions.  
253 The normalised elemental mass loss ( $NL_i$ ) and normalised dissolution rate ( $NR_i$ , 28 days) data  
254 are shown in Tables 4 and 5, respectively. The solution pH buffered to a value of  $pH\ 10.2 \pm 0.2$   
255 after 3 days (Fig. 4) and there was no further measurable fluctuation of pH during the 28-day  
256 duration of the experiments.

257 The normalised elemental loss rates (to 28 days) for boron were similar for each glass  
258 composition, giving an  $NR_B$  between  $3.24 \times 10^{-2} \text{ g m}^{-2} \text{ d}^{-1}$  and  $3.33 \times 10^{-2} \text{ g m}^{-2} \text{ d}^{-1}$  ( $\pm 5 \times 10^{-4}$ )  
259 as stated in Table 4. This indicates that varying the waste loading from 10 to 20 wt% did not  
260 appreciably alter the chemical durability on the timescales investigated. Importantly, the  
261 glasses showed a comparable normalised mass loss and normalised dissolution rate to other  
262 high-level waste glass compositions destined for long-term disposal, tested under comparable  
263 conditions (Table 5). For example, the UK HLW MW25 glass, has a  $NR_B$  of  $3.20 \times 10^{-1} \text{ g m}^{-2} \text{ day}^{-1}$   
264 [33], compared with  $3.24 \times 10^{-2} \text{ g m}^{-2} \text{ d}^{-1}$  for the 20 wt% loaded simulant PFR raffinate glass  
265 (Table 5). The  $NR_B$  is approximately twice that of the SON68 French HLW base glass, however  
266 it should be noted that the specific activity in R7T7 (the active analogue of SON68) will be  
267 substantially higher than that of the PFR loaded G73 glasses. At production, R7T7 contains an  
268 average specific activity ca.  $110 \text{ PBq m}^{-3}$ , approximately 20 times greater than the average ca.

269 6 PBq m<sup>-3</sup> estimated for the G73-20 glass [34]. As such, these glasses could be considered  
270 suitable for the immobilisation and disposal of PFR raffinate.

271 Glass dissolution was observed to be incongruent; B and Na leached at similar rates ( $NL_B >$   
272  $NL_{Na}$ ), however the normalised mass loss of all other elements was an order of magnitude  
273 lower than both B and Na (Table 4). The normalised mass loss of all elements was observed  
274 to be rapid for the first 3 days of dissolution and, after this time, the normalised mass loss of  
275 Si, Na, B began to reduce indicating an approach to quasi-equilibrium, as indicated in Figure  
276 4.

277 The normalised mass loss of Ba and Ca differed as a function of glass composition, albeit  
278 without a notable trend. For example, the normalised mass loss of Ba decreased after 7 days  
279 for the 20 wt% waste loaded composition, and after 14 days for the 15 wt% glass (Fig. 4b).  
280 There appeared to be little removal of Ba from solution from the 10 wt% loaded glass.  
281 Additionally, the  $NL_{Sr}$  dropped after 14 days for all three glasses (Fig. 4f). This behaviour may  
282 be attributed to the formation of Ca-, Ba- and Sr-containing alteration layers on the glass  
283 surface. Indeed, geochemical modelling indicated that tobermorite ( $Ca_5Si_6H_{11}O_{22.5}$ ) is likely to  
284 precipitate. A number of recent investigations have also identified this phase in glasses  
285 containing Ca, or where Ca is present in solution [35–39] and have shown that its formation  
286 can significantly reduce the dissolution rate of nuclear waste glasses, by an order of  
287 magnitude compared to other media [39]. Other phases shown by geochemical modelling to  
288 be favourable precipitates were the Ca- Ba- and Sr-carbonate phases, calcite ( $CaCO_3$ ),  
289 witherite ( $BaCO_3$ ) and strontianite ( $SrCO_3$ ). Arising from equilibrium of  $CO_2$  in air with the  
290 leaching medium, it is possible that these phases precipitated in solution, and when the  
291 samples were filtered for analysis, they were removed, leading to an apparent decrease in Ca,  
292 Ba and Sr leaching. It will be necessary to perform further monolith leaching experiments to

293 examine the properties of the altered layer so that the origin of the fluctuations in these  
294 elements can be determined and set in the context of recent mechanistic studies of UK HLW  
295 and ILW glass performance [40-43].

## 296 **4 - Discussion**

297 Previous work has shown that cement may not have the capacity to effectively immobilise  
298 the diverse inventory of radioactive elements present in the PFR raffinate waste stream [44].  
299 Cementitious wastefoms could be subject to increased dissolution and release rates due to  
300 their inherent porosity and high internal surface area. The high solubility and potential for  
301 removal of many of the waste elements which sorb to the cement surface; especially Cs,  
302 which makes up over 60% of the radioactive inventory by activity, is of potential concern [2].  
303 These factors highlight the opportunity to vitrify PFR wastes to minimise radioisotope  
304 migration to the biosphere. Vitrification, using G73 barium silicate glass described in this  
305 investigation, is likely to offer significant improvements in long term wasteform performance  
306 over the current baseline.

307 The benefits of vitrification reach beyond the improvements in wasteform quality described  
308 and may also offer fiscal incentives, for example, by substantially reducing the waste volumes  
309 for storage and disposal. The current lifecycle waste management plan is to cement the PFR  
310 raffinate in 500 L drums, with a target waste loading of 0.305 m<sup>3</sup> per drum. With 212.1 m<sup>3</sup> of  
311 raffinate to process this would result in 397 m<sup>3</sup> of packaged waste for disposal (696 x 500 L  
312 drums with a displacement volume of 0.57 m<sup>3</sup> each) [2]. If vitrification, at 20 wt% loading was  
313 to be utilised, the volume of waste produced would be reduced to < 14.4 m<sup>3</sup> of glass.  
314 Conceivably, this volume of material could be readily processed in a small or modular plant,

315 utilising one of a variety of thermal treatment options for ILW being developed in the UK e.g.  
316 plasma vitrification, resistive heating melters or Hot-Isostatic Pressing [45].  
317 Assuming packaging of vitrified PFR waste into 3 m<sup>3</sup> ILW boxes was preferable and 70% of the  
318 box capacity (2.57 m<sup>3</sup>) could be filled, each 3 m<sup>3</sup> box would hold 1.8 m<sup>3</sup> of vitrified product. In  
319 this scenario, the waste could be fully conditioned using just eight 3 m<sup>3</sup> boxes, producing a  
320 total waste volume for disposal of 28.6 m<sup>3</sup>. This treatment methodology, when compared  
321 with cementation, would reduce the waste disposal inventory by more than 90%, and, in  
322 principle, could be achieved, using in-container Joule heated melter technology. The heat  
323 generation, surface activity limits and containment limits for impact of this hypothetical G73-  
324 20 waste stream have been estimated to be within existing guidelines for a 3 m<sup>3</sup> ILW box<sup>1</sup>  
325 [46]. The substantial volume reduction achieved by the vitrification approach would enable  
326 transfer of the resulting waste packages to the Sellafield site for storage, potentially assisting  
327 earlier closure of the Dounreay site.  
328 Deriving a lifetime waste management cost for these wastes intended for near surface  
329 storage has not been attempted here. However, it is believed the cost reductions associated  
330 with managing lower volumes of wastes in the rest of the NDA estate should be transferable  
331 to Scottish policy. It is important to note that the volume reduction and concentration of the  
332 waste associated with this vitrification step would not result in the re-classification of the  
333 waste as HLW. This is important as a reclassification to HLW would require consideration of  
334 heat dissipation in storage, introducing significant extra costs for disposal, as well as  
335 increasing the final volume required in a storage vault.

---

<sup>1</sup> Calculation based upon reported inventory of radioisotopes for this waste stream and accounting for the concentration of activity achieved by vitrification. This packaged waste will meet stated specifications imposed for a square corner 3 m<sup>3</sup> box.

336 The decreased risk to public health, superior quality of final wasteform, improved long term  
337 stability, smaller footprint on the Dounreay ILW stores and the reduced waste management  
338 cost, combine to provide a credible case for treatment of these wastes using vitrification over  
339 cementation.

## 340 **5 - Conclusion**

341 A vitreous wasteform for simulant PFR raffinate was developed at a range of waste loadings  
342 up to 20 wt%. The product was a stable and homogeneous amorphous solid with no  
343 observable crystal formation. All glasses performed comparably to vitrified waste  
344 compositions currently in use, both in the UK and internationally, for the immobilisation of  
345 HLW. The aqueous durability was superior to that of current UK HLW glasses under  
346 comparable experimental conditions. Therefore, the glasses investigated here could be  
347 considered a stable matrix for ILW under both geological disposal and near-surface storage  
348 scenarios. The mechanical properties of the wasteform also matched or exceeded those  
349 currently in use for HLW glasses, in both the UK and USA, and therefore, should be amenable  
350 to transport and storage in either 500 L HLW flasks or 3 m<sup>3</sup> ILW waste packages. Additionally,  
351 we demonstrated that undertaking immobilisation of PFR raffinate through thermal  
352 treatment methods may also result in a decrease in the anticipated volume of waste from  
353 397 m<sup>3</sup> to 28.6 m<sup>3</sup>, potentially resulting in significant lifetime waste management cost savings  
354 and a more robust option to support the Scottish policy for at near surface storage and site  
355 closure.

## 356 **Acknowledgements**

357 The authors would like to thank Paul Lythgoe and Alastair Bewsher (School of Earth Science,  
358 University of Manchester) for performing the XRF and ICP-AES measurements presented in

359 this work, Martina Klinkenberg and Jülich Forschungszentrum for access to the FEI SEM. This  
360 research was performed in part at the MIDAS Facility, at the University of Sheffield, which  
361 was established with support from the Department of Energy and Climate Change. We are  
362 grateful to EPSRC for sponsorship of this research under grants EP/G037140/1,  
363 EP/N017870/1, and EP/N017374/1.

## 364 **References**

- 365 [1] S.E. Jensen, P.L. Ølgaard, Description of the prototype fast reactor at Dounreay,  
366 NKS/RAK-2(95)TR-C 1, Rise National Laboratory, Roskilde, Denmark, NKS, 1996.  
367 [http://www.iaea.org/inis/collection/NCLCollectionStore/\\_Public/28/026/28026107.pdf](http://www.iaea.org/inis/collection/NCLCollectionStore/_Public/28/026/28026107.pdf)  
368 (accessed January 7, 2017).
- 369 [2] Nuclear Decommissioning Authority, Waste Stream 5B01 - PFR Raffinate, UK Radioactive  
370 Waste Inventory, (2014).
- 371 [3] K.F. Langley, B.A. Partridge, M. Wise, Immobilization of Fast Reactor First Cycle Raffinate,  
372 in: Proceedings of Waste Management - Tuscon AZ, 2003.  
373 <http://www.wmsym.org/archives/2003/pdfs/50.pdf> (accessed January 7, 2017).
- 374 [4] United Kingdom Atomic Energy Authority (UKAEA), Justification for Classifying PFR  
375 Raffinate as ILW, DSRPTC (2003) P11, (2003).
- 376 [5] United Kingdom Atomic Energy Authority (UKAEA), How To Deal with the Management  
377 of Prototype Fast Reactor (PFR) Raffinate, UKAEA/PP/P(2004)01, (2004).
- 378 [6] United Kingdom Atomic Energy Authority (UKAEA), Best Practicable Environmental  
379 Option Study For The Management of PFR Raffinate, D3900(04)P027, (2005).
- 380 [7] Nuclear Decommissioning Authority, Waste Stream 5B04 - MTR Raffinate, UK  
381 Radioactive Waste Inventory, (2014).
- 382 [8] Nuclear Decommissioning Authority, Waste Stream 5B05 - DFR Raffinate, UK Radioactive  
383 Waste Inventory, (2014).
- 384 [9] J.H. Sharp, J. Hill, N.B. Milestone, E.W. Miller, Cementitious Systems for Encapsulation of  
385 Intermediate Level Waste, in: Proceedings of ICEM '03: The 9th International Conference  
386 on Radioactive Waste Management and Environmental Remediation, Oxford, UK, 2003.
- 387 [10] F. P. Glasser, Mineralogical Aspects of Cement in Radioactive Waste Disposal,  
388 Mineralogical Magazine. 65 (2001) 621–633.
- 389 [11] N.B. Milestone, Y. Bai, C.H. Yang, X.C. Li, The Use of Activated Slags as Immobilisation  
390 Matrices for ILW, in: MRS Online Proceedings Library, 2008: p. 93.
- 391 [12] Committee on Radioactive Waste Management (CoRWM), Response to Scotland's Policy  
392 on Higher Activity Radioactive Waste: Consultation on an Implementation Strategy,  
393 CoRWM document .3220, (2015).
- 394 [13] Scottish Government, Consultation on an Implementation Strategy for Scotland's Policy  
395 on Higher Activity Radioactive Waste, (2015).

- 396 [14] E.R. Merz, D. Dyckerhoff, R. Odoj, Characterization of radioactive wastes incorporated in  
397 a cement matrix, in: Proceedings of International Conference on Radioactive Waste  
398 Management, 1986: pp. 396–401.
- 399 [15] H.J. Mockel, R.H. Koster, Gas Formation During the Gamma Radiolysis of Cemented Low-  
400 and Intermediate-Level Waste Products, NT. 59 (1982) 494–497.
- 401 [16] N.E. Bibler, Radiolytic gas production from concrete containing Savannah River Plant  
402 waste, Du Pont de Nemours (E.I.) and Co., 1978.  
403 [http://inis.iaea.org/Search/search.aspx?orig\\_q=RN:9389931](http://inis.iaea.org/Search/search.aspx?orig_q=RN:9389931) (accessed February 9,  
404 2017).
- 405 [17] C. A Utton, I. H. Godfrey, Review of stability of cemented grouted ion-exchange  
406 materials, sludges and flocs January, (2010).  
407 [https://rwm.nda.gov.uk/publication/review-of-stability-of-cemented-grouted-ion-](https://rwm.nda.gov.uk/publication/review-of-stability-of-cemented-grouted-ion-exchange-materials-sludges-and-flocs-january-2010/)  
408 [exchange-materials-sludges-and-flocs-january-2010/](https://rwm.nda.gov.uk/publication/review-of-stability-of-cemented-grouted-ion-exchange-materials-sludges-and-flocs-january-2010/) (accessed February 9, 2017).
- 409 [18] P.A. Bingham, N. C. Hyatt, R. J. Hand, C.R. Wilding, P.A. Bingham, N.C. Hyatt, R.J. Hand,  
410 C.R. Wilding, Glass Development for Vitrification of Wet Intermediate Level Waste  
411 (WILW) from Decommissioning of the Hinkley Point 'A' Site, MRS Online Proceedings  
412 Library, 1124 (2008) 1124-Q03-07., in: MRS Online Proceedings Library, 2008: pp. Q03-  
413 07.
- 414 [19] P.A. Bingham, N.C. Hyatt, R.J. Hand, Vitrification of UK intermediate level radioactive  
415 wastes arising from site decommissioning: property modelling and selection of  
416 candidate host glass compositions, Glass Technology – European Journal of Glass Science  
417 & Technology Part A, 53, 2012, 83-100.
- 418 [20] P.A. Bingham, N.C. Hyatt, R.J. Hand, S.D. Forder, Vitrification of UK intermediate level  
419 radioactive wastes arising from site decommissioning. Initial laboratory trials, Glass  
420 Technology – European Journal of Glass Science & Technology Part A, 54, 2013, 1-19.
- 421 [21] O.J. McGann, P.A. Bingham, R.J. Hand, A.S. Gandy, M. Kavcic, M. Zitnik, K. Bucar, R. Edge,  
422 N.C. Hyatt,., The Effects of  $\gamma$ -radiation on Model Vitreous Wasteforms Intended for the  
423 Disposal of Intermediate and High Level Radioactive Wastes in the United Kingdom,  
424 Journal of Nuclear Materials. 429 (2012) 353–367.
- 425 [22] C.P. Kaushik, R.K. Mishra, P. Sengupta, A. Kumar, D. Das, G.B. Kale, K. Raj, Barium  
426 borosilicate glass – a potential matrix for immobilization of sulfate bearing high-level  
427 radioactive liquid waste, Journal of Nuclear Materials. 358 (2006) 129–138.
- 428 [23] B. Brendebach, M.A. Denecke, G. Roth, S. Weisenburger, Sulfur incorporation in high level  
429 nuclear waste glass: A S K-edge XAFS investigation, J. Phys.: Conf. Ser. 190 (2009)  
430 012186.
- 431 [24] C.H. Oh, Hazardous and radioactive waste treatment technologies handbook, CRC Press,  
432 2001.
- 433 [25] C 1285-02 Standard Test Methods for Determining Chemical Durability of Nuclear,  
434 Hazardous, and Mixed Waste Glasses and Multiphase Glass Ceramics: The Product  
435 Consistency Test (PCT), ASTM International, (2008).
- 436 [26] A.J. Connelly, R.J. Hand, P.A. Bingham, N.C. Hyatt, Mechanical properties of nuclear  
437 waste glasses, Journal of Nuclear Materials. 408 (2011) 188–193.
- 438 [27] M. Asano, T. Kou, Y. Mizutani, Vaporization of Alkali Borosilicate Glasses, Journal of Non-  
439 Crystalline Solids. 112 (1989) 381–384.
- 440 [28] B.G. Parkinson, Influence of Composition on Structure and Caesium Volatilisation from  
441 Glasses for HLW Confinement, The University of Warwick, 2007.

- 442 [29] J. E. Shelby, *An Introduction to Glass Science and Technology*, 2nd ed., The Royal Society  
443 of Chemistry, Cambridge, 2005.
- 444 [30] R. Short, Phase Separation and Crystallisation in UK HLW Vitrified Products, *Procedia*  
445 *Materials Science*. 7 (2014) 93–100. doi:10.1016/j.mspro.2014.10.013.
- 446 [31] M.H. Langowski, J.G. Darab, P.A. Smith, Volatility literature of chlorine, iodine, cesium,  
447 strontium, technetium, and rhenium; technetium and rhenium volatility testing, Pacific  
448 Northwest Lab., 1996. [http://inis.iaea.org/Search/search.aspx?orig\\_q=RN:27054276](http://inis.iaea.org/Search/search.aspx?orig_q=RN:27054276)  
449 (accessed January 13, 2017).
- 450 [32] I.W. Donald, B.L Metcalfe, R.N.J. Taylor, The Immobilization of High Level Radioactive  
451 Wastes Using Ceramics and Glasses, *Journal of Materials Science*. 32 (1997) 5851–5887.
- 452 [33] H.U. Zwicky, B. Grambow, C. Magrabi, E.T. Aerne, Corrosion Behaviour of British Magnox  
453 Waste Glass in Pure Water, *MRS Online Proceedings Library*. 127 (1988) 127–129.
- 454 [34] L. Wang, *Advances in Transport Phenomena: 2009*, Springer Science & Business Media,  
455 2009.
- 456 [35] C. A. Utton, R. J. Hand, N. C. Hyatt, S. W. Swanton, S. J. Williams, Formation of alteration  
457 products during dissolution of vitrified ILW in a high-pH calcium-rich solution. *Journal of*  
458 *Nuclear Materials*, 4421, 33 – 45, 2013, *Journal of Nuclear Materials*. 4421 (2013) 33–  
459 45.
- 460 [36] S. Mercado-Depierre, F. Angeli, F. Frizon, S. Gin, Antagonistic effects of calcium on  
461 borosilicate glass alteration, *Journal of Nuclear Materials*. 441 (2013) 402–410.
- 462 [37] S. Gin, P. Jollivet, M. Fournier, C. Berthon, Z. Wang, A. Mirtoshkov, Z. Zhu, J. V. Ryan, The  
463 fate of silicon during glass corrosion under alkaline conditions: A mechanistic and kinetic  
464 study with the International Simple Glass, *Geochimica et Cosmochimica Acta*. 151 (2015)  
465 68–85.
- 466 [38] C.A. Utton, S.W. Swanton, J. Schofield, R.J. Hand, A. Clacher, N.C. Hyatt, Chemical  
467 durability of vitrified wastefoms: effects of pH and solution, *Mineralogical Magazine*, 76  
468 (2012), 2919-2930.
- 469 [39] C. L. Corkhill, N. J. Cassingham, P. G. Heath, N. C. Hyatt, Dissolution of UK high level waste  
470 glass under simulated hyperalkaline conditions of a co-located geological disposal  
471 facility, *International Journal of Applied Glass Science*. 4 (2013) 341–356.
- 472 [40] N. Cassingham, C.L. Corkhill, D.J. Backhouse, R.J. Hand, J.V. Ryan, J.D. Vienna, N.C. Hyatt,  
473 The initial dissolution rates of simulated UK Magnox-ThORP blend nuclear waste glass as  
474 a function of pH, temperature and waste loading, *Mineralogical Magazine*, 79, 2015,  
475 1529-1542.
- 476 [41] H. Zhang, C.L. Corkhill, P.G. Heath, R.J. Hand, M.C. Stennett, N.C. Hyatt, Effect of Zn- and  
477 Ca oxides on the structure and chemical durability of simulant alkali borosilicate glasses  
478 for immobilisation of UK high level wastes, *Journal of Nuclear Materials*, 462, 2015, 321-  
479 328.
- 480 [42] N.J. Cassingham, C.L. Corkhill, M.C. Stennett, R.J. Hand, Alteration layer formation of Ca-  
481 and Zn-oxide bearing alkali borosilicate glasses for immobilisation of UK high level waste:  
482 A vapour hydration study, *Journal of Nuclear Materials*, 479, 2016, 639-646.
- 483 [43] N.C. Hyatt, R.R. Schwarz, P.A. Bingham, M.C. Stennett, M. C. C.L. Corkhill, P.G. Heath, R.J.  
484 Hand, M. James, A. Pearson, S. Morgan, Thermal treatment of simulant plutonium  
485 contaminated materials from the Sellafield site by vitrification in a blast-furnace slag,  
486 *Journal of Nuclear Materials*, 444, 2014, 186-199.
- 487 [44] M. Atkins, F. P. Glasser, Application of Portland Cement-Based Materials to Radioactive  
488 Waste Immobilization, *Waste Management*. 12 (1992) 105–131.

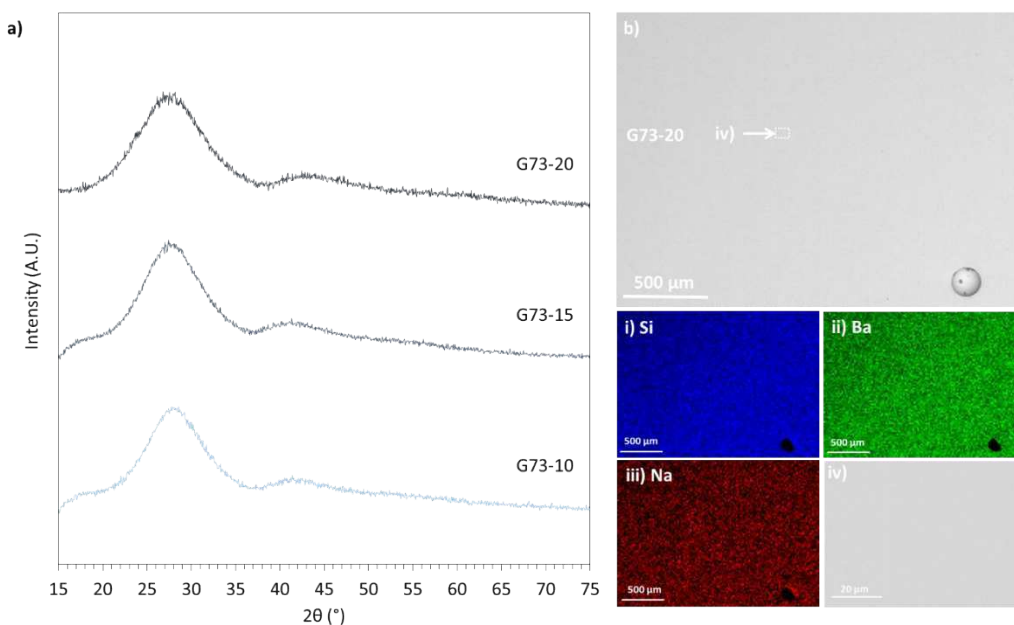
489 [45] N.C. Hyatt, M. James, Thermal treatment of ILW, Nuclear Engineering International. 58  
490 (2013) 10–13.

491 [46] G. Steele, Areva Risk Management Consulting, Contents Activity for the Square Corner 3  
492 m<sup>3</sup> Box Waste Package Transported in an SWTC-285 Transport Container, NDA.RWMD.  
493 R07-023(C) J6214.23, (2009).

494

495

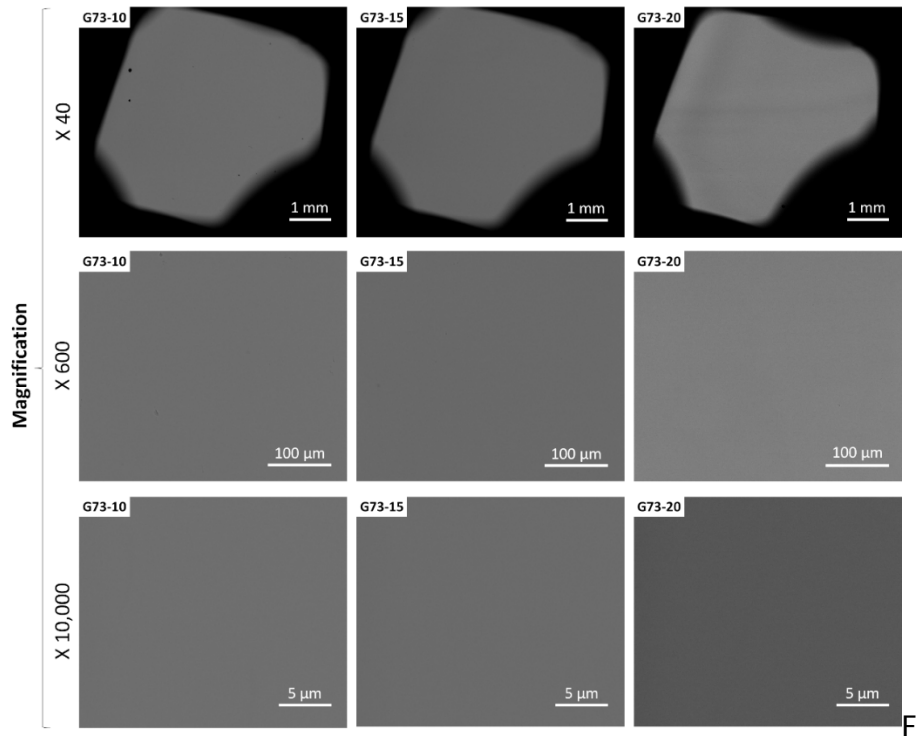
496 **Figures**



497

498 **Figure 1 - a) Powder XRD patterns of G73 PFR raffinate loaded glasses, displaying diffuse scattering characteristic of**  
499 **amorphous material and b) SEM-BSE image displaying homogeneity of G73-20 glass matrix, set above i) - iii) SEM-EDX**  
500 **maps of key elements for b) and iv) a higher resolution BSE-SEM of G73-20 glass matrix identified in b) which taken**  
501 **illustrates the absence of crystalline materials in the final waste product.**

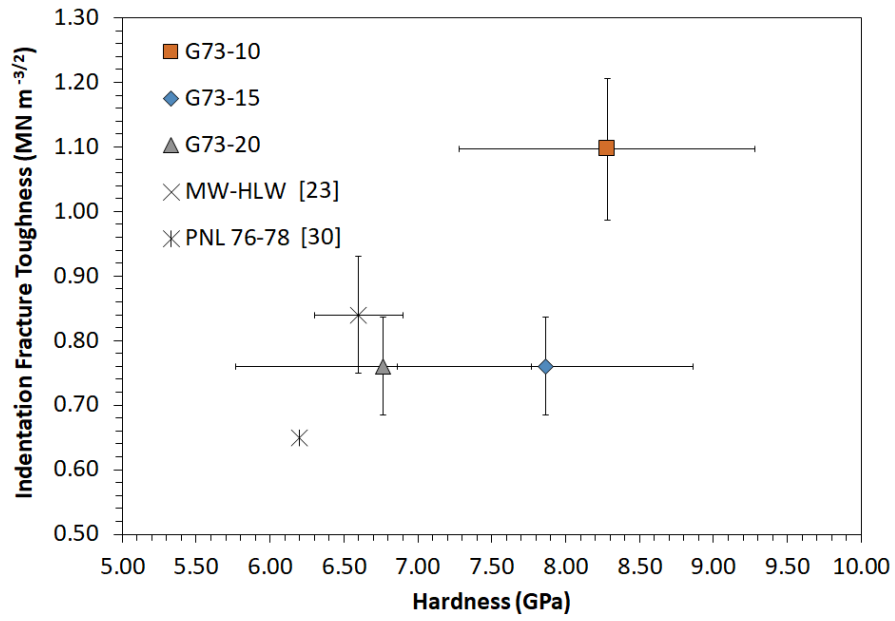
502



503

504 Figure 2 - SEM-BSE images of the three waste loaded glasses G73-10, G73-15 and G73-20 at various magnifications. The  
 505 lack of image contrast suggests chemical homogeneity within the sample.

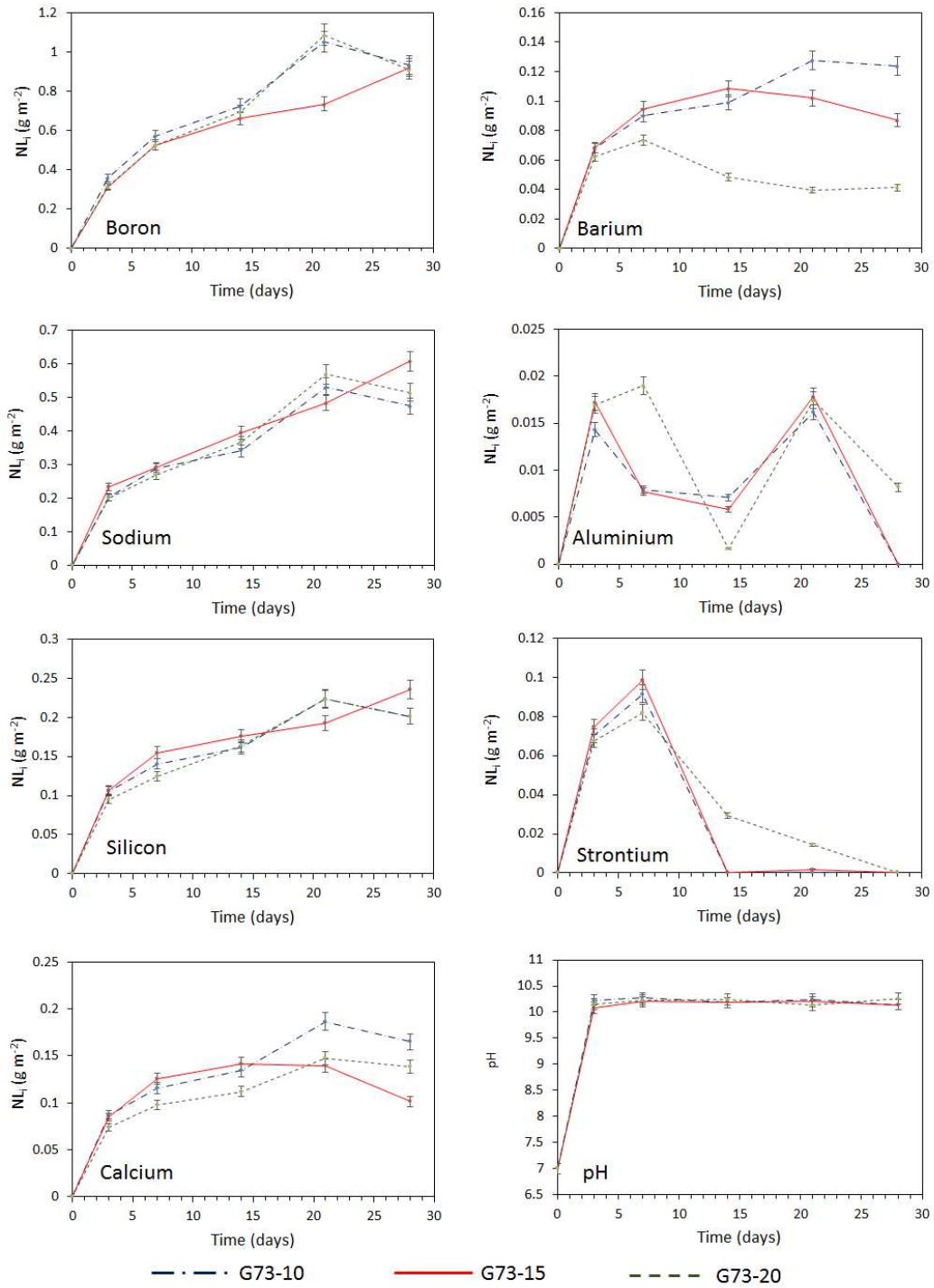
506



507

508 **Figure 3 - Indentation fracture toughness and hardness values of G73 PFR raffinate waste loaded glasses obtained using**  
 509 **the Vickers indentation methodology, with comparison to waste glasses currently used for HLW immobilisation [23,30].**  
 510 **Errors correspond to 3 x the measured standard deviation.**

511



512

513 Figure 4 - Graphs displaying the normalised elemental mass loss with varying levels of PFR raffinate loading from PCT  
 514 experiments at 90°C in 18.2 MΩ water with a SA/V of 1499 m<sup>-1</sup>-1525 m<sup>-1</sup> (dependant on glass density).

515

516 **Tables**

Included in Simulant (surrogate element used)		Excluded from Simulant	
<i>Element</i>	<i>ppm</i>	<i>Element</i>	<i>ppm</i>
<i>Na</i>	9,711	<i>Rh</i>	15
<i>Cu</i>	8,725	<i>Cm</i>	4
<i>Fe</i>	3,837	<i>Nb</i>	3.5
<i>Zn</i>	3,566	<i>Dy</i>	2.4
<i>Cd</i>	2,540	<i>Ag</i>	<1.3
<i>S</i>	1,351	<i>As</i>	<13
<i>Ni</i>	1,277	<i>Co</i>	<0.4
<i>Cr</i>	669	<i>Ge</i>	<1.3
<i>Cs</i>	509	<i>Hg</i>	<0.3
<i>Nd</i>	462	<i>Ho</i>	<1.3
<i>Am (Sm)</i>	405	<i>In</i>	<4
<i>Al</i>	350	<i>Np</i>	<13
<i>Ce</i>	304	<i>P</i>	<2.7
<i>U (Ce)</i>	168	<i>Pb</i>	<1.1
<i>La</i>	163	<i>Rb</i>	<1.3
<i>Pr</i>	158	<i>Sb</i>	<1.3
<i>Mo</i>	154	<i>Se</i>	<1.3
<i>Pd</i>	150	<i>Sn</i>	<0.3
<i>Ca</i>	138	<i>Tc</i>	<1.3
<i>Sm</i>	123	<i>Eu</i>	15
<i>Y</i>	112	<i>Gd</i>	15
<i>Te</i>	74	<i>Pd</i>	150
<i>Sr</i>	60		
<i>Mn</i>	45		
<i>Ru</i>	60		
<i>Ba</i>	39		
<i>Ti</i>	36		
<b>Total</b>	<b>35,186</b>	<b>Total</b>	<b>205</b>

517 **Table 1 - Average composition of PFR raffinate as characterised in [6]. (Brackets) indicate where the use of an appropriate**  
518 **inactive simulant was applied. The right-hand columns identifies elements excluded from the simulant based on both low**  
519 **concentrations in the raffinate and on an economic basis.**

520  
521  
522

Table 2 - Compositions of base glass, simulant calcined PFR raffinate and glasses produced. Compositions of glasses provided both as batched and as measured by XRF (boron analysis via dissolution in HF and ICP-AES). \*Note glasses were batched to 100 wt%; discrepancies reported result from rounding to 2 d.p.

Component (wt%)	G73-00 Base Glass	PFR Calcine	G73-10		G73-15		G73-20	
			Batch	Meas.	Batch	Meas.	Batch	Meas.
SiO <sub>2</sub>	42.0	0.00	37.80	34.29	35.70	33.4	33.60	32.58
BaO	42.0	0.09	37.81	41.21	35.71	41.61	33.62	38.61
Fe <sub>2</sub> O <sub>3</sub>	6.00	11.68	6.57	7.88	6.85	7.78	7.14	7.56
CaO	5.00	0.41	4.54	4.55	4.31	4.54	4.08	4.40
Na <sub>2</sub> O	2.50	27.88	5.04	1.64	6.31	2.38	7.58	3.30
CuO	0	26.26	2.63	2.83	3.94	3.98	5.25	5.05
B <sub>2</sub> O <sub>3</sub>	2.00	0.00	1.80	0.46	1.70	0.56	1.60	0.46
ZnO	0	9.45	0.95	1.08	1.42	1.55	1.89	1.93
CdO	0	6.18	0.62	0.74	0.93	1.05	1.24	1.35
SO <sub>3</sub>	0	7.18	0.72	0.72	1.08	0.79	1.44	0.86
Al <sub>2</sub> O <sub>3</sub>	0.50	1.41	0.59	0.86	0.64	0.85	0.68	1.2
NiO	0	3.46	0.35	0.55	0.52	0.71	0.69	0.86
Cr <sub>2</sub> O <sub>3</sub>	0	2.08	0.21	0.48	0.31	0.56	0.42	0.66
Cs <sub>2</sub> O	0	1.15	0.12	0.36	0.17	0.42	0.23	0.52
Nd <sub>2</sub> O <sub>3</sub>	0	1.15	0.12	0.15	0.17	0.00	0.23	0.23
Sm <sub>2</sub> O <sub>3</sub>	0	0.30	0.03	0.10	0.05	0.14	0.06	0.19
CeO <sub>2</sub>	0	0.97	0.10	0.05	0.15	0.10	0.19	0.12
MoO <sub>3</sub>	0	0.49	0.05	0.06	0.07	0.08	0.10	0.09
Y <sub>2</sub> O <sub>3</sub>	0	0.30	0.03	0.03	0.05	0.05	0.06	0.06
La <sub>2</sub> O <sub>3</sub>	0	0.04	0.00	0.03	0.01	0.00	0.01	0.04
Pr <sub>6</sub> O <sub>11</sub>	0	0.04	0.00	0.04	0.01	0.06	0.01	0.09
RuO <sub>2</sub>	0	0.17	0.02	0.00	0.03	0.00	0.03	0.00
SrO	0	0.15	0.02	0.6	0.02	0.12	0.03	0.07
TeO <sub>2</sub>	0	0.20	0.02	0.00	0.03	0.00	0.04	0.00
TiO <sub>2</sub>	0	0.13	0.01	0.00	0.02	0.00	0.03	0.00
Mn <sub>2</sub> O <sub>3</sub>	0	0.14	0.01	0.08	0.02	0.08	0.03	0.09
	100	-	100.13	98.795	100.20	100.81	100.26	100.32

524

Glass Property	Sample ID		
	G73-10	G73-15	G73-20
Density (g cm <sup>-3</sup> )	3.512 ± 0.002	3.572 ± 0.002	3.574 ± 0.003
Glass Transition Temperature (°C)	470 ± 10	483 ± 10	484 ± 10
Liquidus Temperature (°C)	1045 ± 10	1075 ± 10	1020 ± 10

525 [Table 3 - Properties of glass wastefoms produced at varying PFR raffinate waste loadings including the density, liquidus](#)  
526 [temperature \(measured in mullite crucibles - see main text for the implication of this\) and glass transition temperature.](#)

527

NR <sub>i</sub> (g m <sup>-2</sup> day <sup>-1</sup> )	Glass Composition		
	G73-10	G73-15	G73-20
B	3.33 x 10 <sup>-2</sup>	3.28 x 10 <sup>-2</sup>	3.24 x 10 <sup>-2</sup>
Na	1.69 x 10 <sup>-2</sup>	2.17 x 10 <sup>-2</sup>	1.84 x 10 <sup>-2</sup>
Si	7.18 x 10 <sup>-3</sup>	8.40 x 10 <sup>-3</sup>	7.19 x 10 <sup>-3</sup>
Ca	5.89 x 10 <sup>-3</sup>	3.62 x 10 <sup>-3</sup>	4.95 x 10 <sup>-3</sup>
Mo	4.44 x 10 <sup>-3</sup>	4.78 x 10 <sup>-3</sup>	6.38 x 10 <sup>-3</sup>
Ba	4.43 x 10 <sup>-3</sup>	3.10 x 10 <sup>-3</sup>	1.47 x 10 <sup>-3</sup>
Cr	3.48 x 10 <sup>-4</sup>	1.64 x 10 <sup>-4</sup>	2.30 x 10 <sup>-4</sup>
Cu	4.93 x 10 <sup>-6</sup>	1.45 x 10 <sup>-6</sup>	0.00
Al	0.00	0.00	2.91 x 10 <sup>-4</sup>
Fe	0.00	0.00	0.00
Ni	0.00	0.00	0.00
Sr	0.00	0.00	0.00
Zn	0.00	0.00	0.00

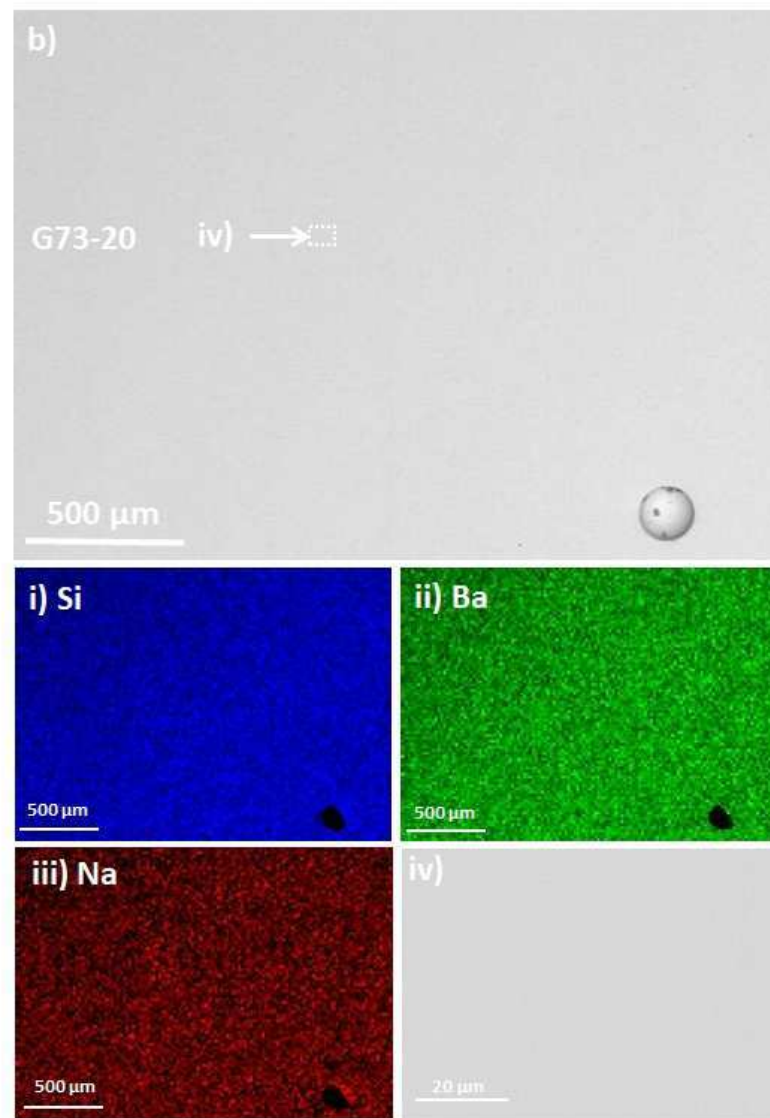
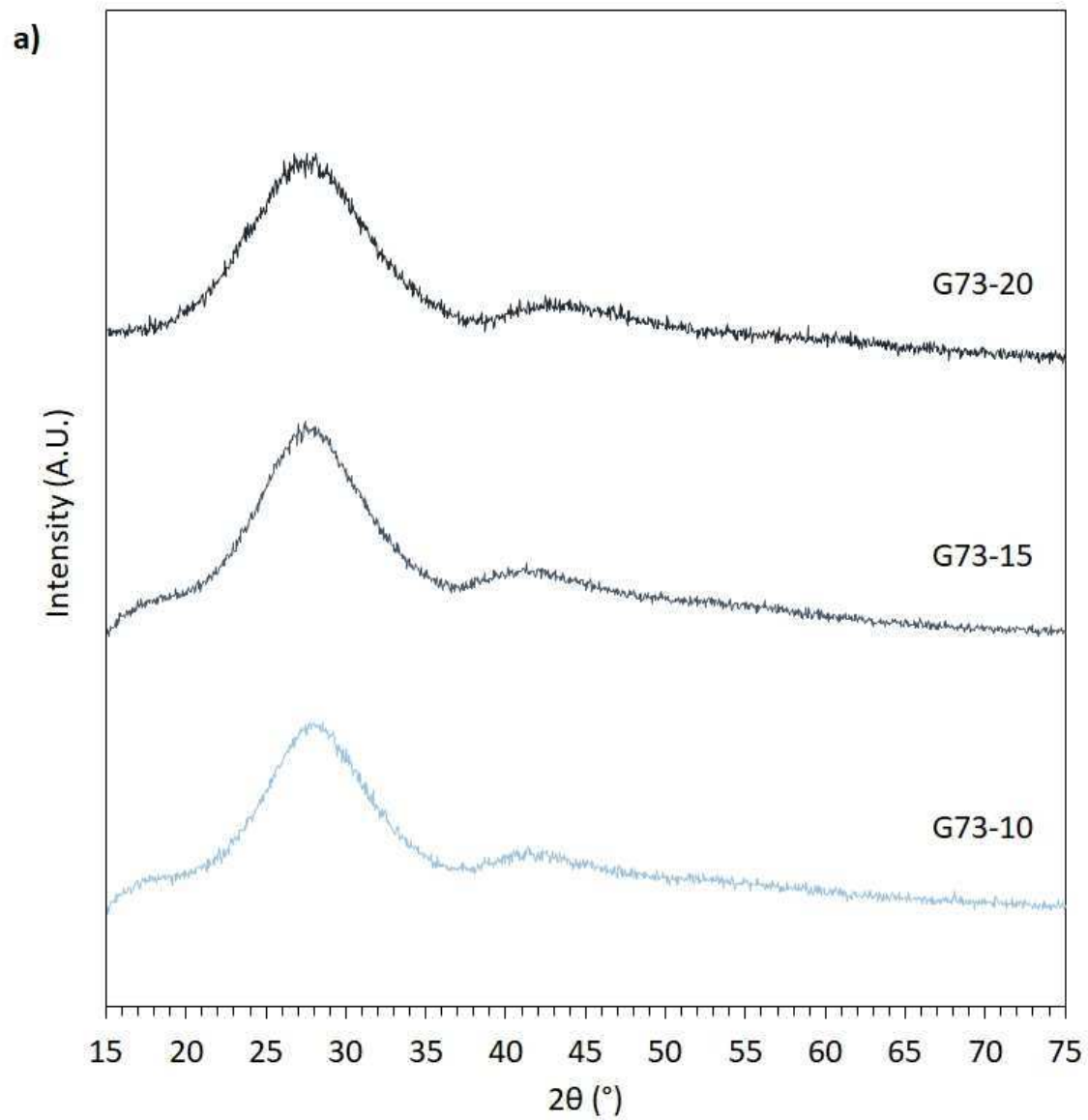
528 Table 4 - Normalised elemental loss rates for the three waste PFR waste loaded glasses measured after 28 days. Data is  
529 from PCT experiments of the wasteforms at 90 °C in 18.2 MΩ water.

530

Glass Composition	NL <sub>i</sub> after 28 days (g m <sup>-2</sup> )		NR <sub>i</sub> after 28 days (g m <sup>2</sup> day <sup>-1</sup> )		SA/V (m <sup>-1</sup> )	pH (25 °C)
	NL <sub>B</sub>	NL <sub>Si</sub>	NR <sub>B</sub>	NR <sub>Si</sub>		
G73-20	0.9076	0.2012	0.0324	0.0072	1499	10.26
SON68 [40]	0.4886	0.1559	0.0175	0.0055	2135	9.4
MW25 [31]	8.89	0.538	0.32	0.020	1200	-

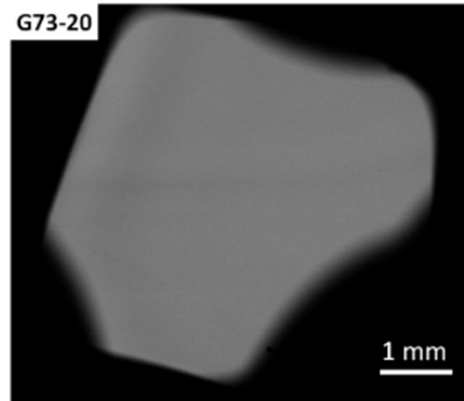
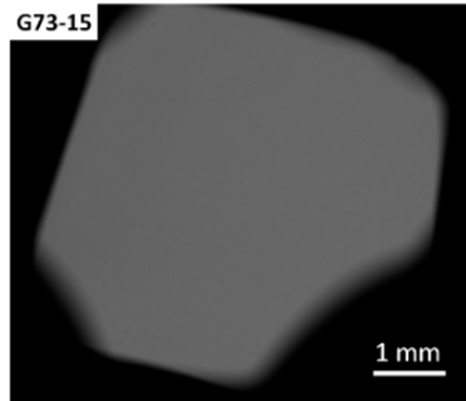
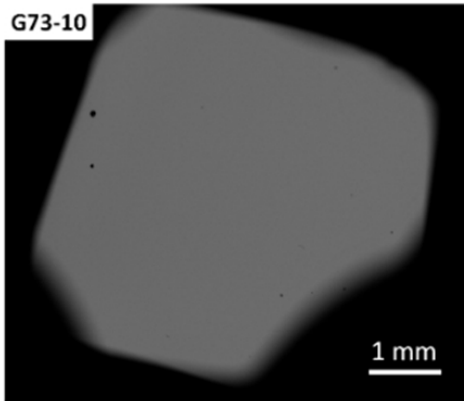
531 Table 5 - Comparison of network dissolution limiting normalised elemental mass losses and normalised elemental  
532 dissolution rates between SON68 glass, British Magnox waste HLW glass and G73-15 waste loaded glasses tested, under  
533 PCT conditions at 90 °C in 18.2 MΩ water.

534

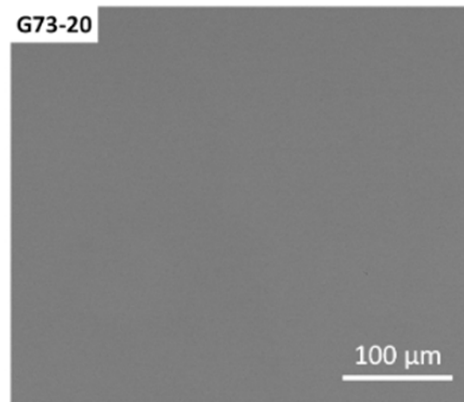
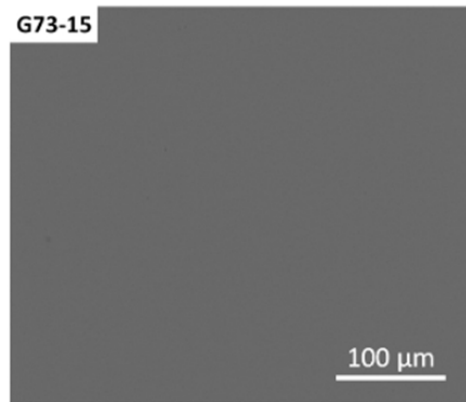
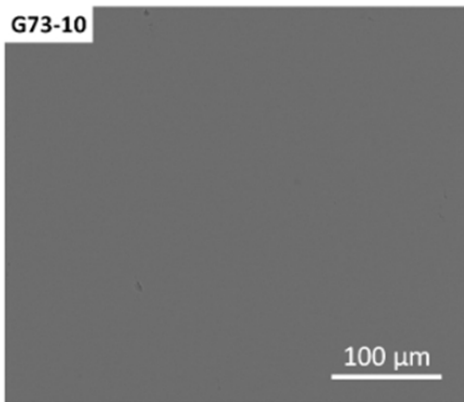


Magnification

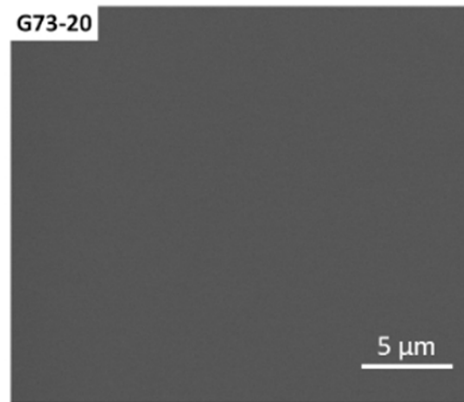
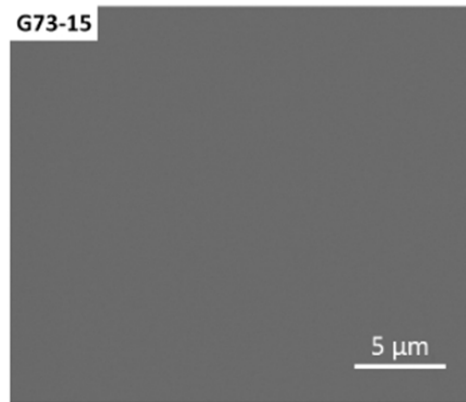
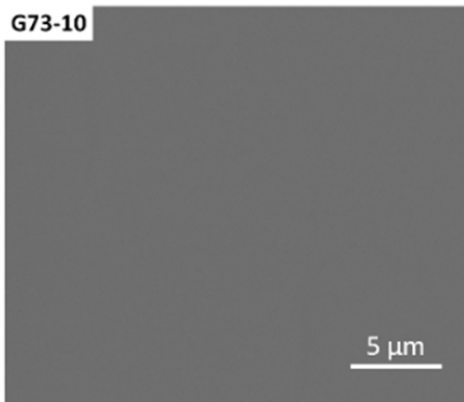
X 40

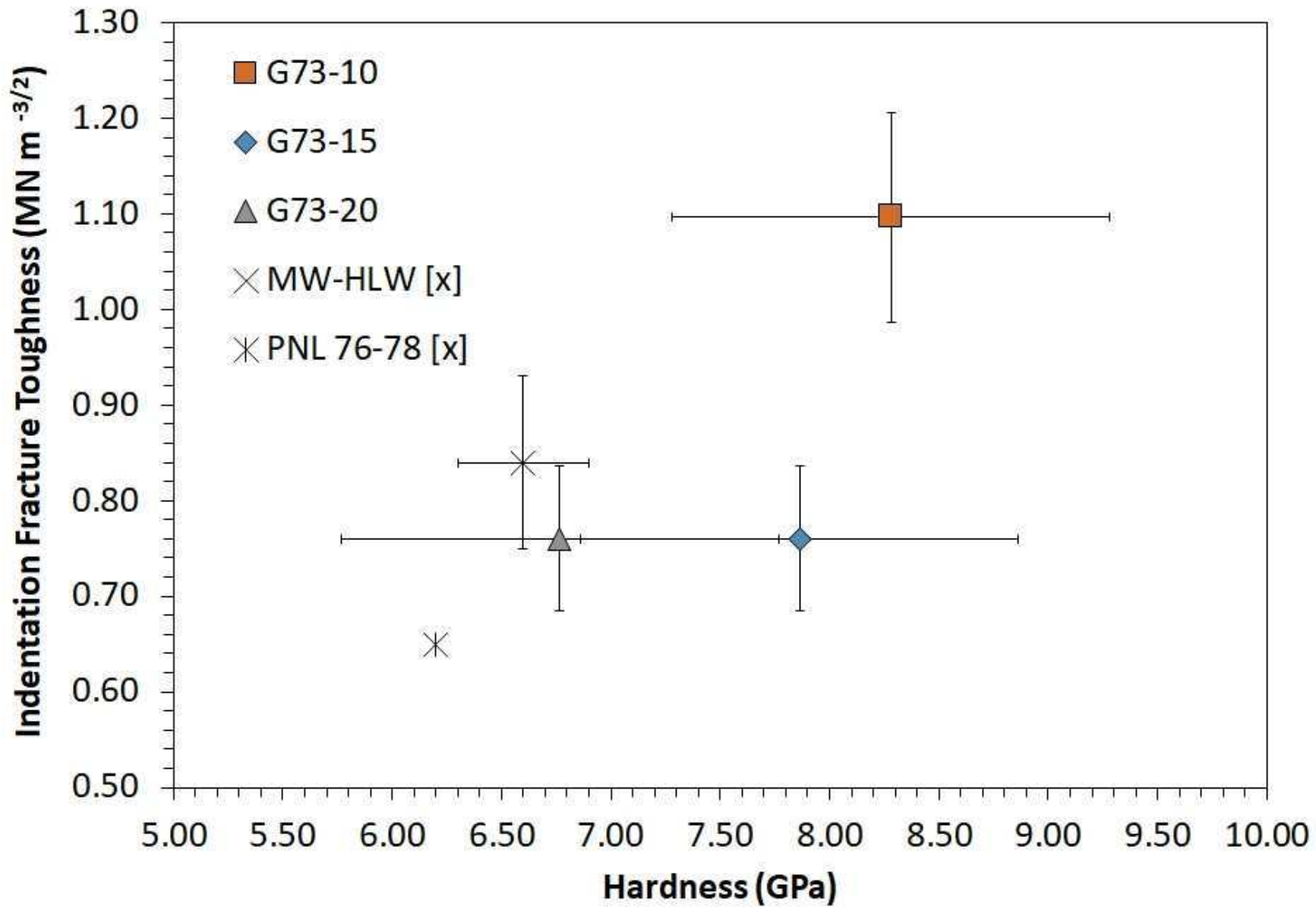


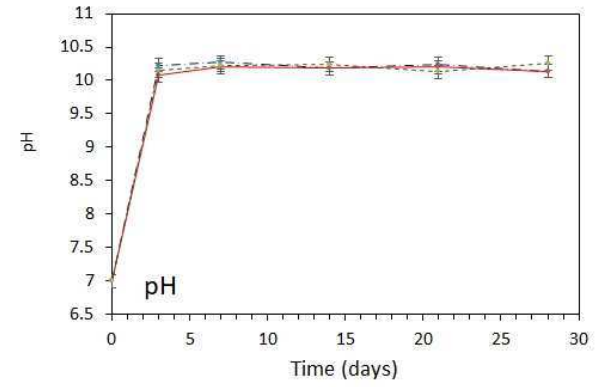
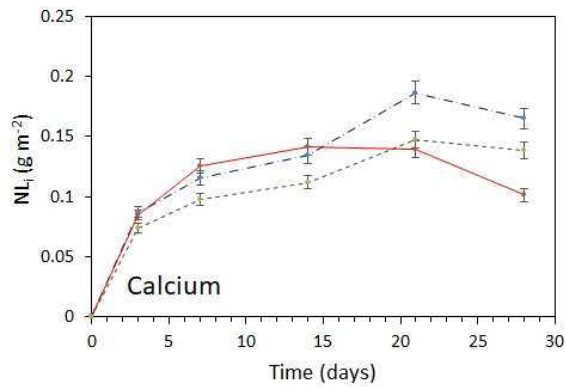
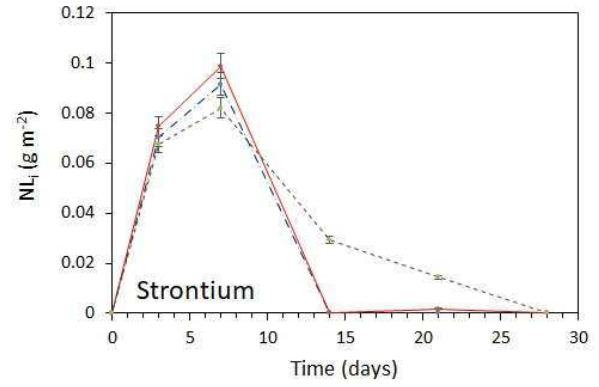
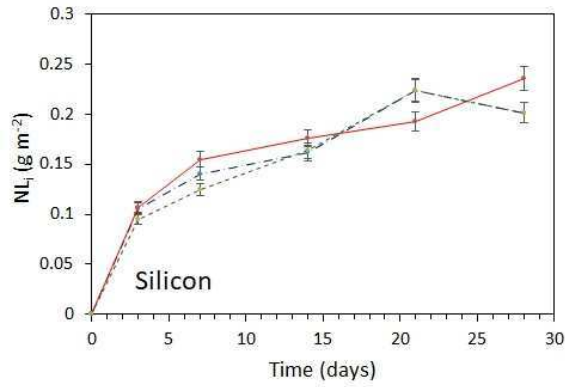
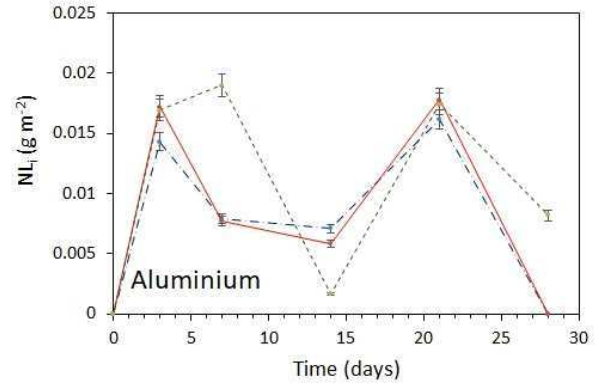
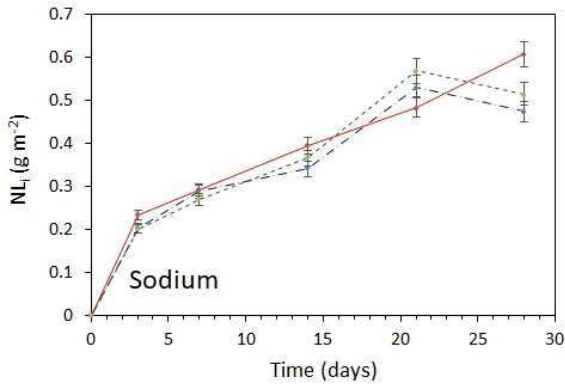
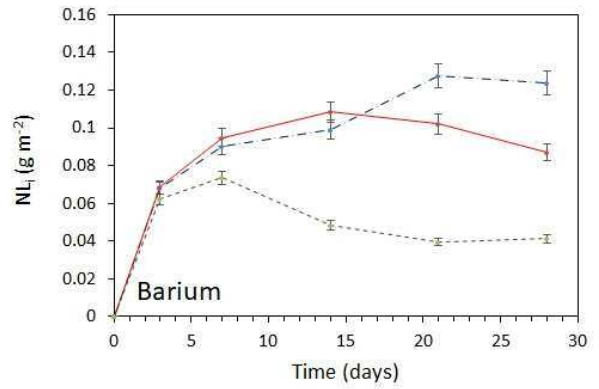
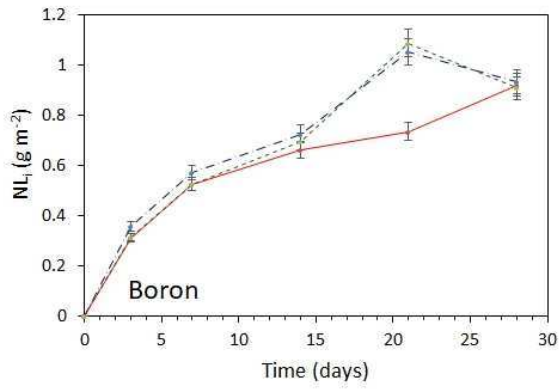
X 600



X 10,000







- · - · - G73-10     
 — G73-15     
 - - - G73-20